



jwst



ESTEC

European Space Research
and Technology Centre
Keplerlaan 1
2201 AZ Noordwijk
The Netherlands
www.esa.int

TECHNICAL NOTE

High-Resolution Modelling of the Spectral MSA Leakage

Prepared by	A. Deshpande
Reference	ESA-JWST-SCI-NRS-TN-2018-007
Issue/Revision	1.0
Date of Issue	August 30, 2018
Status	Draft



APPROVAL

Title High-Resolution Modelling of the Spectral MSA Leakage	
Issue Number 1	Revision Number 0
Author A. Deshpande	Date August 30, 2018
Approved by the boss	Date of Approval whenever

CHANGE LOG

Reason for change	Issue Nr.	Revision Number	Date

CHANGE RECORD

Issue Number 1	Revision Number 0		
Reason for change	Date	Pages	Paragraph(s)

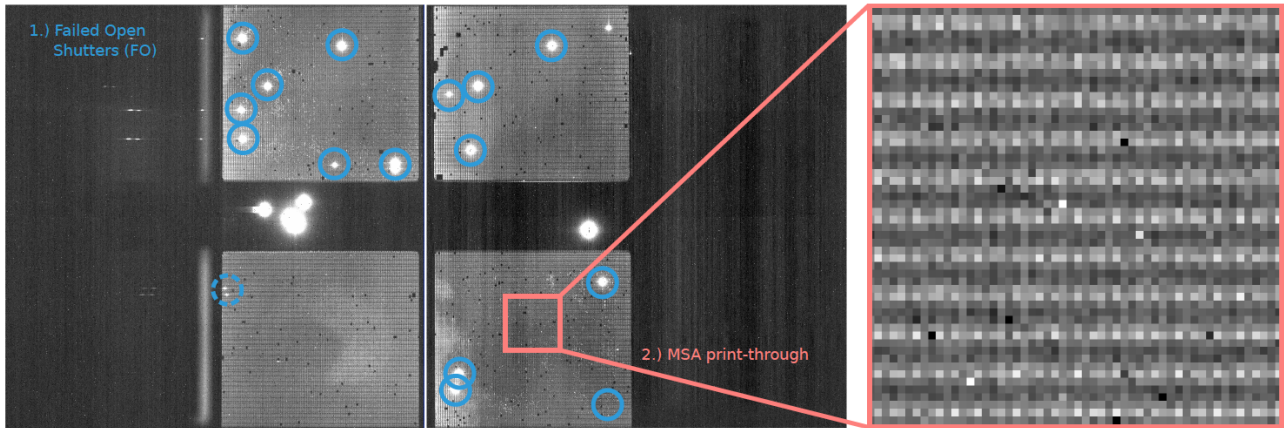
DISTRIBUTION

Name/Organisational Unit
SCI-ODJ
SCI-S
STScI
ESTEC

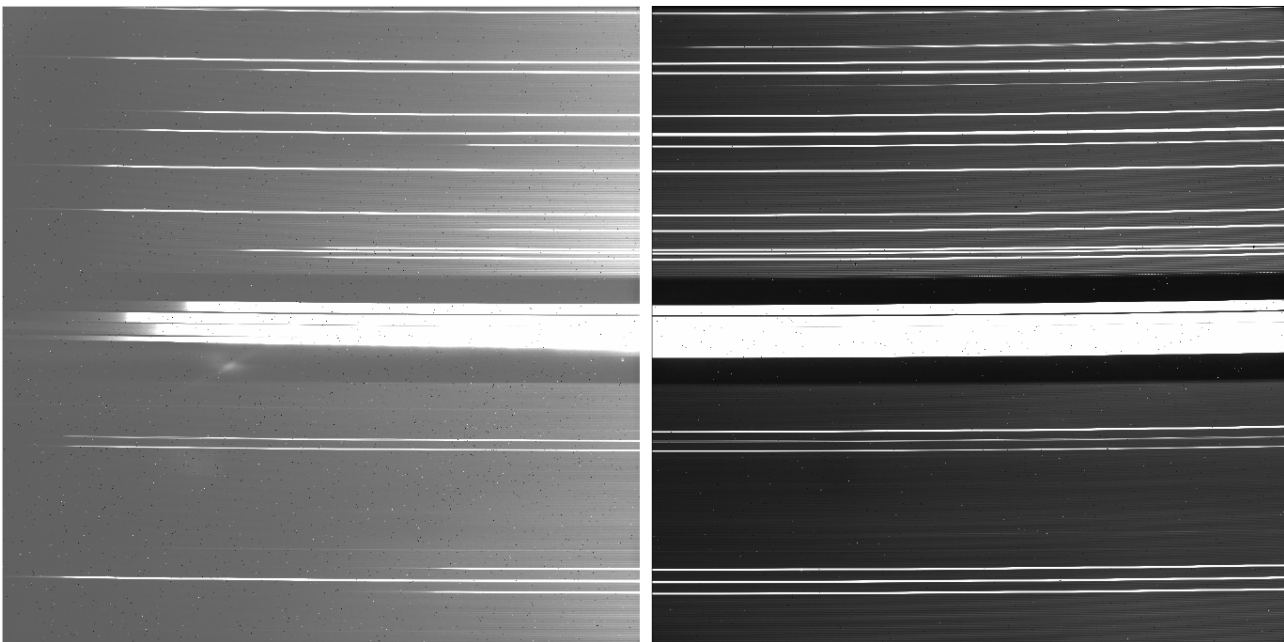


Contents

1	Introduction	5
2	Tracing the Leakage	5
2.1	Mapping the Structure	5
2.2	Scaling for Individual Shutters	6
2.3	A Second Leakage Component	7
3	Modelling the Spectral Leakage	12
3.1	Mapping On-detector Spectra	12
3.2	Simulating a Leakage Exposure	13
4	Testing the Spectral Model	14
4.1	The Prism	14
4.2	G140M	19
4.3	G395H	25
5	Conclusion	31
6	References	32



(a) The parasitic signal seen in imaging mode. This exposure was obtained for configuration MSA=ALLCLOSED, IFU=closed with the internal FLAT lamp. The blue circles highlight FO shutters, whereas the remaining pattern is the leakage. The bright circles in the central region is light from the apertures for the instrument’s fixed slits. (Lützendorf 2017)



(b) When obtaining spectra, this parasitic signal propagates and piles up in the spectral dimension, as shown in this figure. This is ISIM NID 30197 for configuration G140M, MSA=ALLCLOSED, IFU=closed, with lamp FLAT1. This lamp is equivalent to an extended source viewed through F100LP. Again, two distinct features are observed: the bright, pronounced isolated white lines which are signal from individual FO shutters; and the more nebulous, lower magnitude MSA leakage. Similar to 1a, the thick spectra in the central region are from the instrument’s fixed slits.

Figure 1: Exposures illustrating the parasitic signal known as MSA leakage in imaging and spectral modes.

1 INTRODUCTION

The Near Infrared Spectrograph (NIRSpec) is one of the scientific instruments aboard the James Webb Space Telescope (JWST). The instrument possesses several operational modes; Multi-Object Spectroscopy (MOS), Fixed Slit spectroscopy (FS), and Integral Field Spectroscopy (IFS). As a consequence of their spectra sharing the same detector real-estate, observations from the MOS and IFS modes must be mutually exclusive. Consequently, the Micro-Shutter Assembly (MSA), used for MOS, must be fully closed when using the Integral Field Unit (IFU).

However, some light passes through the MSA even when it is fully closed, affecting IFU observations. The MSA's finite, non-ideal contrast creates a parasitic signal; here referred to as 'MSA leakage'. Compounding this is the existence of Failed Open (FO) shutters; defective shutters that are permanently open. These effects are illustrated in Figure 1. A comprehensive assessment of the leakage for all of NIRSpec's instrumental configurations, reveals a level of signal that is typically less than 10% that of observed IFS spectra (Deshpande 2017). In order to better characterize this parasitic signal, and in view of developing a model-based mitigation strategy for IFS observations, a detailed spectral model of the MSA leakage is required. In particular, complications such as the variability of the leakage due to grating wheel re-positioning mean that an over-sampled, higher than detector resolution, model is necessary. It must be noted that these effects are only significant in the detector's spatial axis, and so oversampling is only required in the detector's spatial axis.

Initial attempts to model the leakage signal as it appears in imaging mode, are detailed within ESA-JWST-SCI-NRS-TN-2017-051 (Lützendorf 2017). One of the key challenges demonstrated by this work is the need to achieve a high level of computational efficiency, given the required high resolution of the spectral model. For example, increasing the detector resolution by a factor of 20 requires the computation of $20 \times 4 \times 171 \times 365$ separate spectra. This proves to be an intensive task demanding multiple days of processing time. In this document we discuss an alternate technique of high resolution modelling that aims to bypass this time requirement. We firstly replicate and update this previous work, generating improved oversampled maps of the MSA leakage in imaging mode. Next, we describe the techniques and computational strategies used to produce a time-efficient high resolution spectral model. Finally, we compare simulations obtained from the model with calibration exposures taken during cryo-vacuum ground testing, in order to quantify the model's accuracy.

2 TRACING THE LEAKAGE

2.1 Mapping the Structure

We can map the structure of the leakage by taking an exposure where every operable micro-shutter is closed and the MSA is fully illuminated, in imaging mode. This can be achieved using NIRSpec's internal Calibration Assembly (CAA) lamps, as can be seen in Figure 1a. However, such a detector image greatly undersamples individual shutters, with each shutter only illuminating $\sim 3 \times 5$ detector pixels. To overcome this limitation, one can assume that, to the first order, the structure of the leakage is the same for all shutters and accordingly re-project each shutter onto a common reference frame. Given that there are $\sim 250,000$ shutters available, the re-projection results in a finely sampled map of the leakage from a typical micro-shutter (Lützendorf 2017).

In order to carry out this re-projection, we used the NIRSpec instrument model (Dorner et al. 2016). The generation of the high-resolution shutter map was carried out with the script `L_shutter_normalise.py`, which undertakes the following steps. Initially, a desired resolution is chosen. The script then generates arrays with sizes matching the prescribed resolution. These arrays contain evenly spaced values between -0.5 and 0.5 in shutter pitch x and y coordinates. For our purposes, a resolution of 60 points in the pitch x direction, by 125 points in the pitch y direction was deemed sufficient. The script then iterates through every combination of coordinates formed by these arrays. Using NIPS, the positions on the detector corresponding to a particular set of pitch coordinates, for each shutter, are recorded for a given detector image. Here, we used NID 30398,

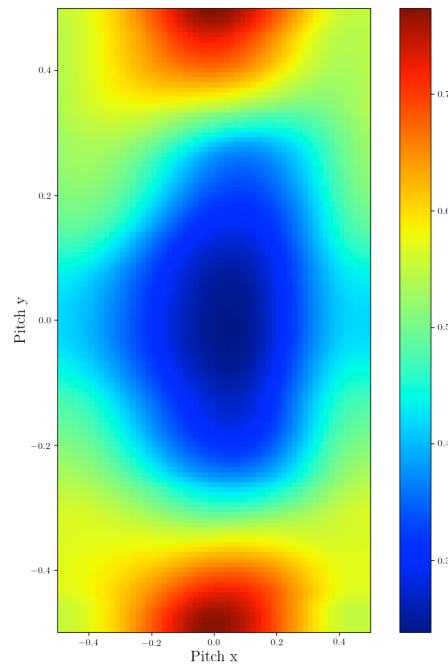


Figure 2: High resolution map of the structure of common MSA leakage across all shutters. Constructed from exposure NID 30398. Each point is the median of the values of the detector pixel corresponding closest to said point, across every shutter. The values displayed are in units of electron count.

obtained using CAA lamp FLAT5. All values at these detector coordinates are collected and, after masking out bad data using the supplied quality flags, their median is taken. This median is then assigned as the value of the corresponding point in the high resolution leakage map. We set any negative values to zero. The shutter map obtained from this approach is given in Figure 2.

2.2 Scaling for Individual Shutters

Figure 1a demonstrates that the contrast of the leakage varies across the MSA. Therefore, while the structure encapsulated in Figure 2 could be considered common to all shutters, scaling to individual shutters is required in order to ensure the model is representative. Whereas in previous modelling attempts, only one scale factor per quadrant was used for this common leakage, this investigation applied individual scaling for each shutter, in an attempt to improve accuracy. The scaling was also performed using `L_shutter_normalise.py`.

An important consideration when scaling is that, as explained in ESA-JWST-SCI-NRS-TN-2017-051 (Lützendorf 2017) and can be seen in Figure 2, the majority of the leakage originates from the bars between the micro-shutters, rather than from the shutter apertures. While the bars of the MSA are coated in a non infrared transparent coating, this coating has interruptions in it, through which light leaks. These interruptions are necessary as the coating is highly conductive, meaning shorts can occur between MSA rows/columns in their absence. However, since shutter pitch coordinates only extend to the halfway points of the bars surrounding a shutter, parts of the leakage are truncated in our maps. So, for each micro-shutter, in order to accurately scale the magnitude of the leakage, we place nine copies of the generic high resolution map together, in a 3×3 grid. In this way, we have a map of the entirety of the leakage from the bars surrounding a particular shutter. This is then rebinned to the detector's resolution; mimicking what a section of a detector image would look like. From an actual leakage exposure, an area corresponding to a 3×3 grid of shutters, centered on the current shutter, is extracted. For this purpose, we again used exposure NID 30398. A least-squares minimization, with one scale factor corresponding to each shutter in the excerpt, is carried out, in order to fit the rebinned model grid to the

extracted detector image grid. The minimized scale factor for the central shutter in the grid is then stored. In the event that the current shutter is on the outermost rim of an MSA quadrant, such that it is not possible to fully cover one or more of the bars, a more rudimentary approach is used. The median value of all the pixels comprising that shutter is found. The median of a single high resolution map is also taken. That shutter’s scale factor is then the ratio of the detector image median to the generated map median.

2.3 A Second Leakage Component

Previous work (Lützendorf 2017) demonstrates that a single shutter map, such as the one constructed in the

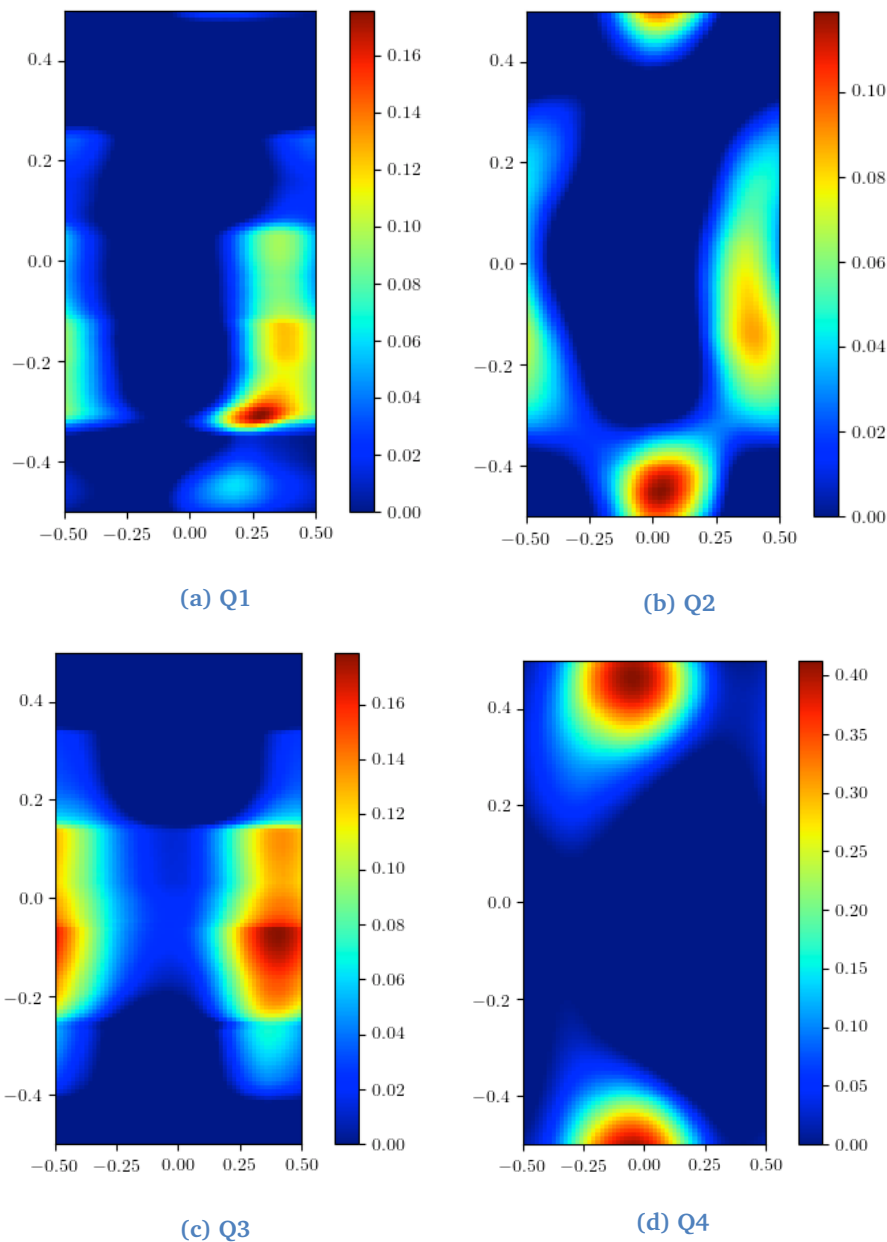
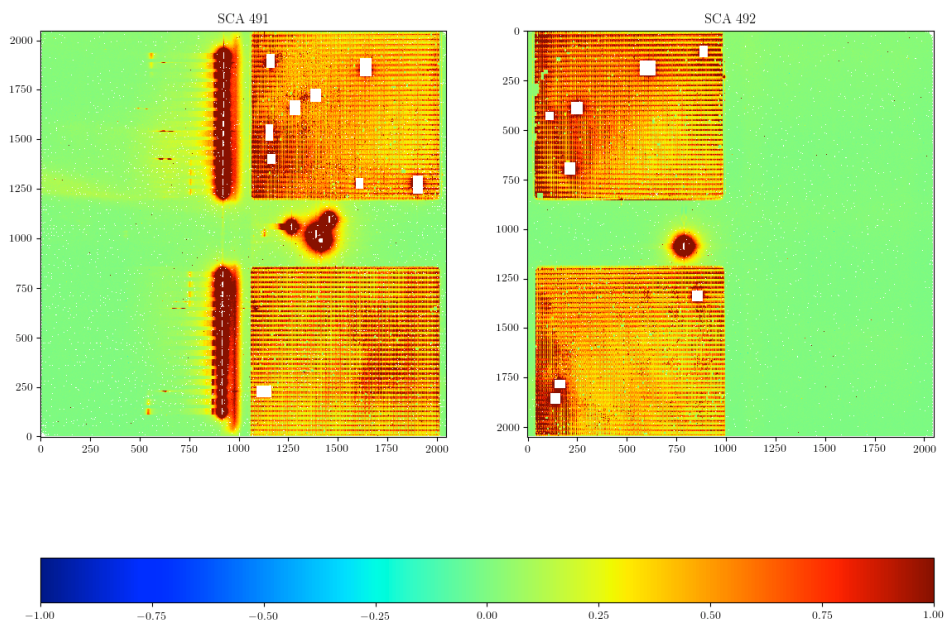


Figure 3: High-resolution maps of a second common form of leakage for each quadrant. These are found after the subtraction of the component shown in Figure 2, and by using the same method of oversampling a detector image. Coordinates are in pitch, and values are in electron count.

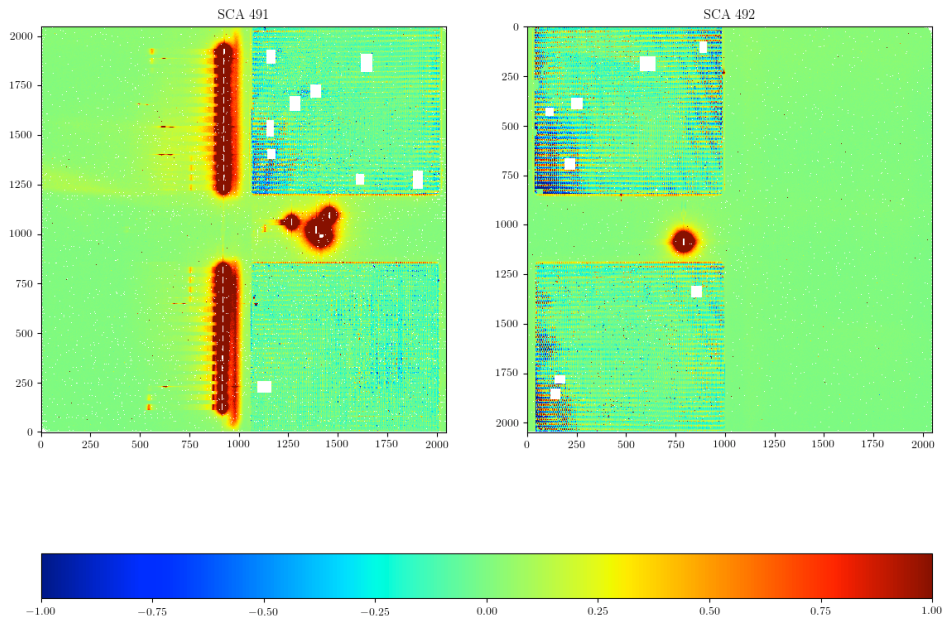
preceding section, does not fully encapsulate the variation in leakage from shutter to shutter. Accordingly, we investigated whether the residuals of the leakage component modeled so far have a common structure.

As an initial step to measuring any potential common second component, we subtracted the first component from the detector image. This was again carried out with `L_shutter_normalise.py`. To begin with, it iterates through each high-resolution pixel of each shutter, then scales its value using the corresponding factor, and identifies the detector pixel corresponding to it. Next, for each detector pixel, all identified and scaled high-resolution points are integrated over. Accordingly, a detector resolution map of the entire MSA is created. This was used to perform the subtraction of the first common leakage component. The oversampling technique used to generate Figure 2, was then applied to this subtracted image, with one key change. Instead of generating a universal map for all shutters, four individual maps corresponding to the four MSA quadrants were generated. These maps were constructed by only sampling the shutters within their respective quadrants. They are displayed in Figure 3.

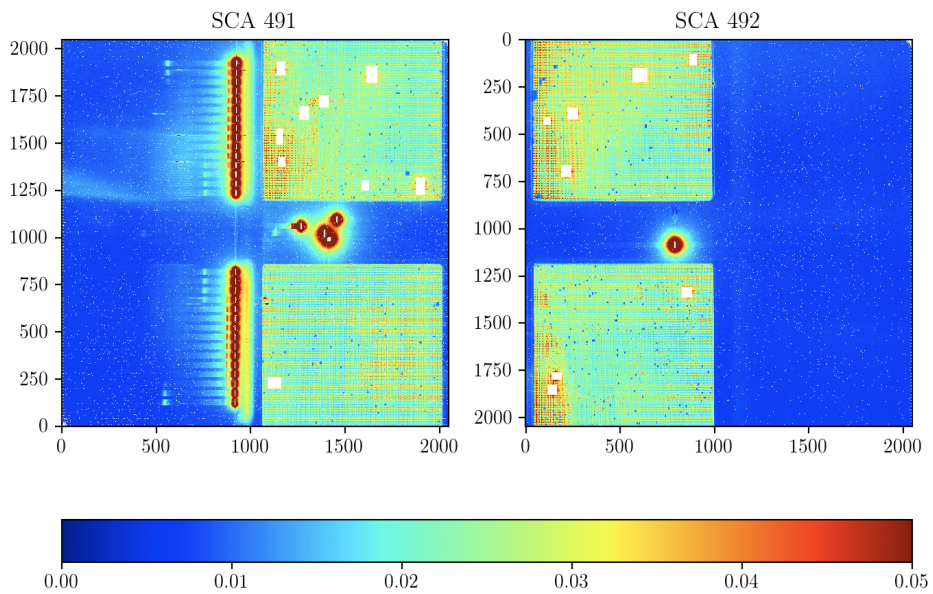
We see that, generally, there is a second common leakage component around the hinge areas and at the borders of where the shutter doors could be expected to be. Although it is somewhat unclear what causes the second type of leakage, it is thought to be due to improperly closed or warped shutter doors. The notable exception to this is MSA Q4, where there appears to be no door leakage. Instead, the technique employed picks up the residuals for the first type of leakage that were not well subtracted. In fact, this is can also be partly seen in MSA Q2. The noticeable difference between each quadrant's map also emphasises the necessity of having four separate maps. As before, these maps then needed to be scaled for individual shutters. This was completed by `L_shutter_normalise.py`, using much the same logic as for the preceding component. However, this time the simple median-to-median method of scaling was used, as the minimization technique did not offer improvements, despite being more computationally expensive. Finally, these new scaled shutter maps were also subtracted from the detector image. The original image, a map of the noise in the image, and an image of the residuals after the full subtraction are shown below, in Figure 4. Figure 5 shows the results of carrying out the full model subtraction, for verification purposes, on a second exposure of the MSA; one not used in the construction of the model. Histograms showing the distribution of values before and after subtraction, for both these cases, are in Figure 6. Histograms of the residuals for each quadrant individually, in the cases of both subtractions, are given in Figure 7. These residuals seem largely consistent with each other, as well as those reported in ESA-JWST-SCI-NRS-TN-2017-051 (Lützgendorf 2017).



(a) MSA leakage in imaging mode, NID 30398.



(b) Residuals of subtraction of leakage models from image NID 30398.



(c) Noise levels in image NID 30398.

Figure 4: Image of the MSA leakage before and after subtraction, and noise levels in image, for all MSA quadrants. FO shutters are masked, along with all pixels with non-ideal quality flags. In all cases, values are in electron counts.

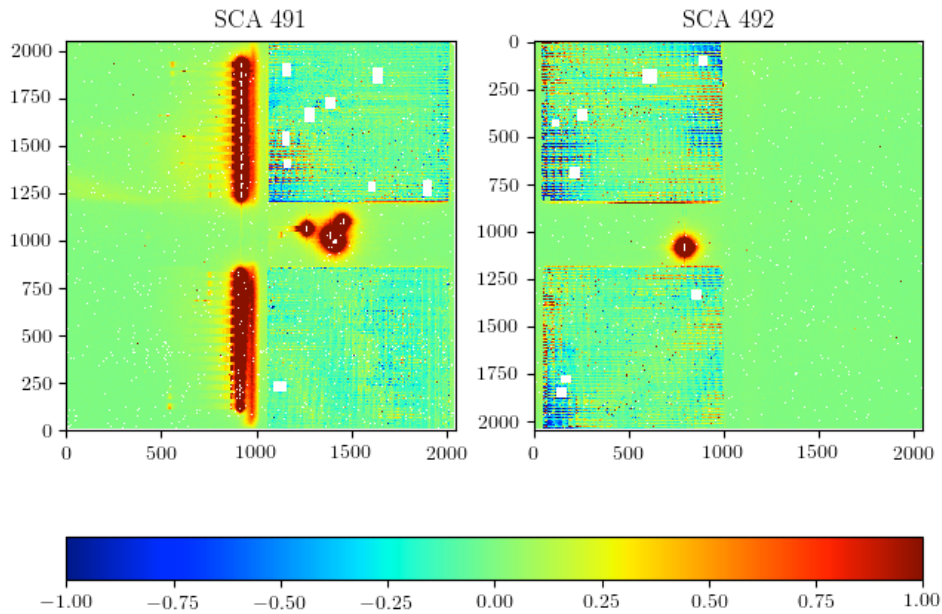
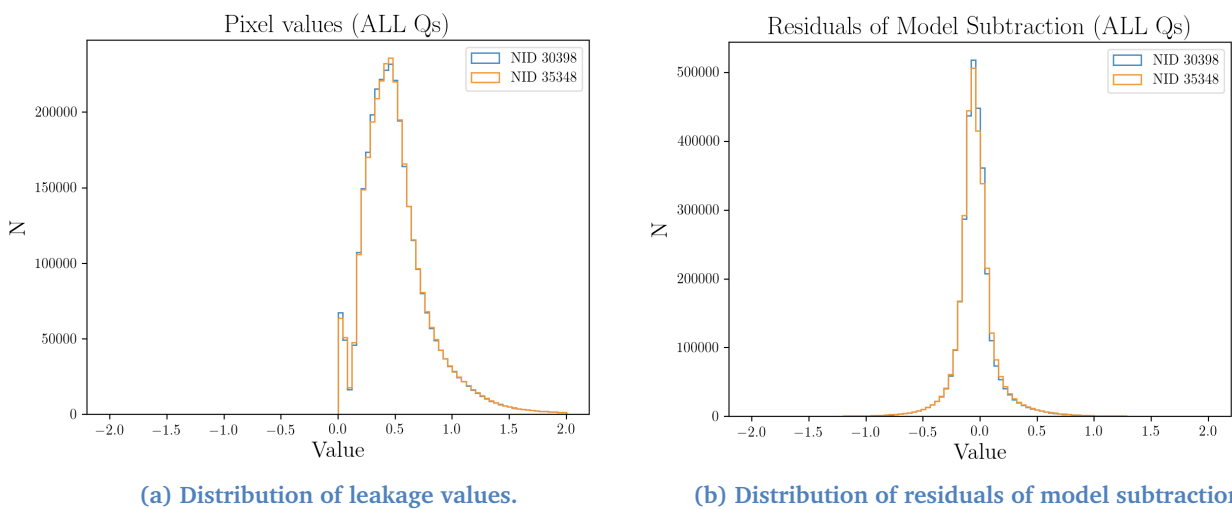


Figure 5: Residuals of subtraction of leakage models from image NID 35348.



(a) Distribution of leakage values.

(b) Distribution of residuals of model subtraction.

Figure 6: Histograms displaying the distribution of electron count values in two detector images, before and after the total subtraction of the model.

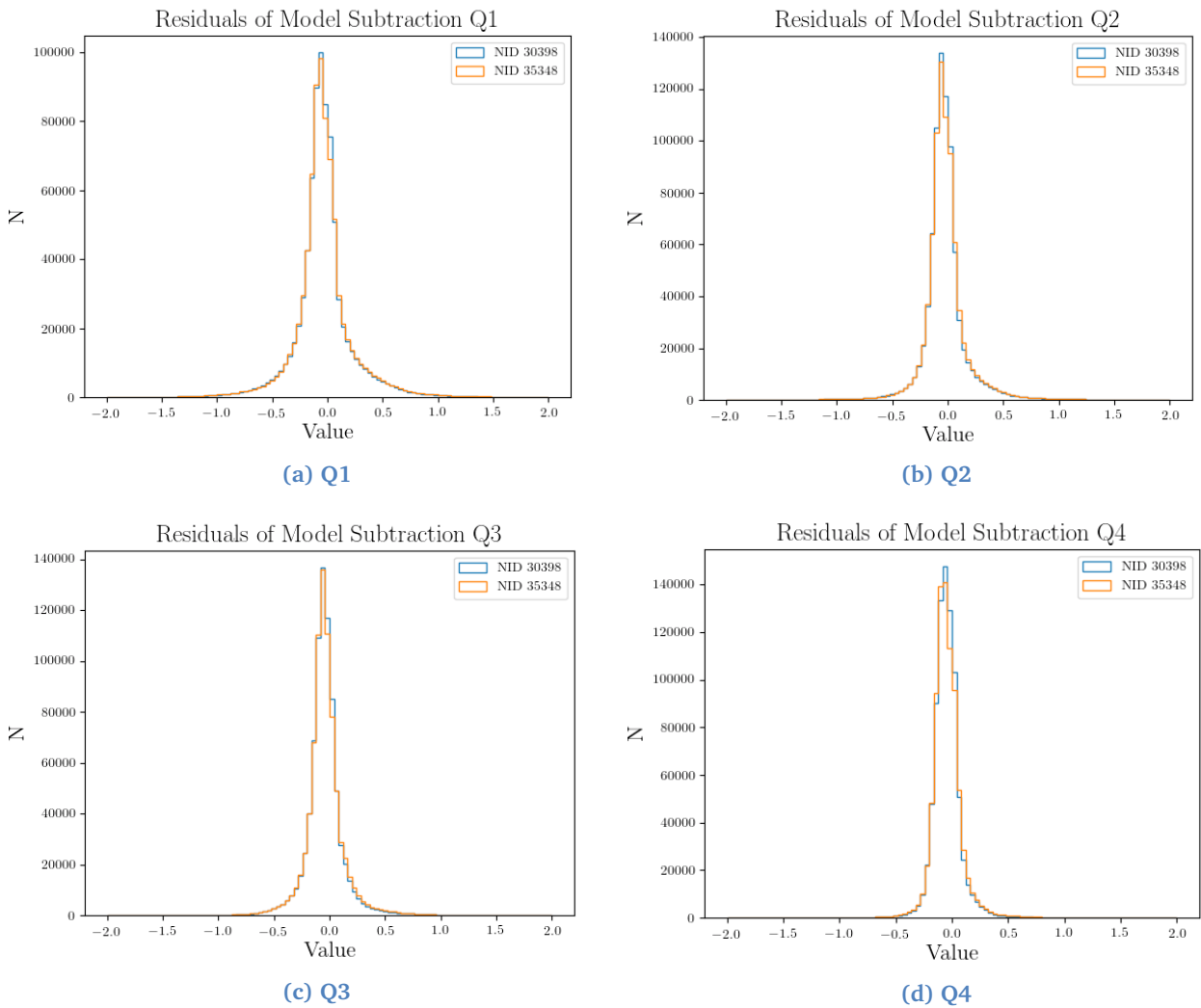


Figure 7: Histograms showing the individual residuals after model subtraction for each MSA quadrant. Values are in electron counts.

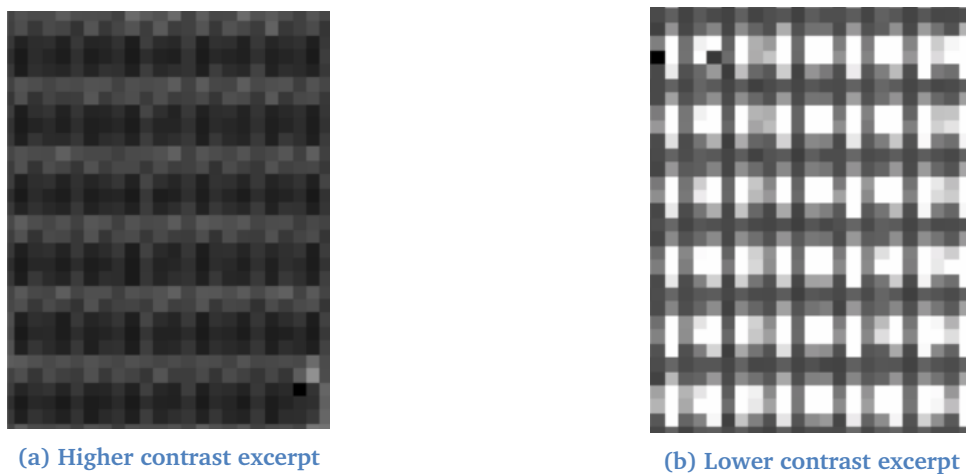


Figure 8: Lower and higher contrast sections from Q3 of exposure NID 30398.

From Figures 4 and 5, we see that the regions where the subtraction is worse correspond to areas of the MSA with generally higher values of leakage; on the fringes of quadrants. We also observe, in Figure 4c, that these areas of the actual image have higher levels of noise. Closer examination of these areas reveals that the imprint of the leakage differs here in comparison to the better subtracted regions of the MSA. This is evident in Figure 8. Essentially, the obtained shutter maps are less representative here as, for the lower contrast regions, the light appears to leak more through the central regions of the shutter, as opposed to the bars and hinges. To complicate matters, a unique high-resolution shutter map cannot be constructed for just these regions because it is difficult to designate a non-arbitrary criteria to identify all the applicable shutters, and we may not have enough different shutters per quadrant to achieve the required resolution. However, the remnant residuals can be used to improve the accuracy of the model. Using `L_shutter_normalise.py`, we extracted and stored the individual residuals for each shutter.

3 MODELLING THE SPECTRAL LEAKAGE

3.1 Mapping On-detector Spectra

It would be possible to disperse the leakage models derived in the previous sections using the NIRSpec Instrument Pipeline Software (NIPS). However, this approach is prohibitively time-consuming to be repeated each time a new simulation is required. To minimize the impact of this constraint, we adopted an approach where this computation was only required once. For each of NIRSpec's dispersers, we calculated and stored relationships that identify the wavelengths and positions within an MSA shutter traveled through for all the light corresponding to a given set of detector coordinates.

These relationships were computed using the script `L_relation.py`. Bivariate interpolation was used to compute the required functions. Given that different wavelengths passing through different shutters can end up falling on the same detector pixel it was, in principle, necessary to compute a separate transformation relationship for each shutter. Fortunately, the spectra of the shutters in a particular column do not overlap, simplifying the problem to a degree. Instead of having $365 \times 171 \times 4$ relationships to compute, we could simply have 365×4 ; one for each column in every quadrant. One function per column does not conflict with the high-resolution requirement because the higher resolution is only required in the detector's spatial axis, not its spectral one.

In detail, for a particular disperser, `L_relation.py` starts off by creating an array of wavelengths covering that disperser's operational range, with a sampling matching the resolution of the detector in the spectral direction. It then iterates through each column of shutters in the MSA, performing the following procedure: Using NIPS, each wavelength from the array is projected onto the detector through multiple points, in the pitch y direction, within every shutter in the column. For each individual combination, four parameters are recorded: the specific position in the column that was used, the particular wavelength, and the resulting detector i and j coordinates. Next, A bivariate spline based interpolation is carried out to generate a function which can go from detector coordinates, to location in column and wavelength. The recorded data for a column is fed into the `scipy.interpolate` library's `bisplrep` routine. Our requirement in this investigation was to be able to oversample the detector by a maximum factor of 20, in the spatial direction. To get functions out of this process that are accurate enough to within $1/20^{\text{th}}$ of a detector pixel, different numbers of points per shutter were needed for each disperser. The number of points used for each disperser are stated in Table 1. In this way, we obtained 365×4 relationships per disperser.

However, while using these interpolated functions proved faster than traversing the entire NIPS pipeline, applying these to the required $20 \times 2048 \times 4242$ oversampled detector pixels still takes upwards of 24 hours even when multi-processed on 32 core system. Accordingly, carrying out these computations on-the-fly each time a new simulation is required is also too expensive. We decided to mitigate this factor by again requiring this computation to be run only once per disperser, at the cost of increased storage. The script `L_model.py` was used to do this, by putting every detector pixel through each of the pre-computed functions and recording the results. A list containing every valid wavelength, MSA location, and detector pixel coordinate combination was

Table 1: Number of points per shutter required for interpolations between detector coordinates, and the corresponding position in an MSA column and wavelength to be accurate to within $1/20^{\text{th}}$ of a detector pixel.

Disperser	Points Per Shutter
G140M	140
G140H	130
G235M	120
G235H	130
G395M	50
G395H	170
PRISM	20

generated. In this way, when creating new simulations, the model only needs to read the list for the appropriate items. However, this approach is not without its flaws, as each disperser's list has a size of ~ 3 TB.

3.2 Simulating a Leakage Exposure

By using the previously generated high resolution shutter maps in conjunction with the lists of leakage positions, an exposure of the spectral MSA leakage for a supplied input spectrum can be simulated. `L_model.py` performs this operation. As a first step, techniques used for 1D modelling of leakage in ESA-JWST-SCI-NRS-RP-2017-002 (Deshpande 2017), in order to establish the Spectral Energy Distributions (SEDs) of the input spectra after passing through a specified instrumental configuration, are adopted. For a selected configuration, the script first computes the wavelength ranges for the zeroth, -1, and -2 orders for the spectrum in MOS mode. For the prism, only the zeroth order is generated. Using `nirspecperf.py`, it also computes the Photon Conversion Efficiency (PCE) for each of the aforementioned orders. Next it takes an input spectrum, and contains it in an instance of the 'Spectrum' class from `spectrum.py`. The various orders for these spectra are calculated, and then re-binned into the pixel resolution of the detector. They are then converted into electron rates by using the PCEs.

Given that oversampling is only required in the spatial direction, the script then takes the shutter level leakage maps from Figures 2 and 3, and rebins them to be only one unit wide in the pitch x direction. At this stage, the values of these maps are still in electron counts. They must be converted into contrast values identifying what fraction of the total light that could fall on a shutter if it was fully open manages to leak through. The total value is calculated by summing over the spectrum if the FLAT5 CAA lamp, which is used to generate exposure NID 30398. Dividing every value in the map by this total value converts it into the required contrast map. This rebinning and scaling process is also applied to the individual residual maps stored for each shutter.

Next, a zeroed array representing the oversampled detector is created. The script then iterates through the previously generated list of wavelength, MSA location, and detector pixel combinations, in order to build the final spectral leakage map. Firstly, for a particular row in the list, it identifies the MSA quadrant, the shutter i and j coordinates within that quadrant, and the pitch y position within the shutter. The appropriate contrast maps and scale factors to be used are identified. The values at the listed pitch in both relevant contrast maps, and the relevant residual map, are taken, multiplied by their corresponding scale factors, and added together. This gives the fraction of any particular light that leaks through from this point in the shutter.

Following on, the wavelength of the current item in the list is compared to previously generated spectrum for the main order of the current disperser. For the gratings, this is order -1, whereas for the prism it is the zeroth order. The currently selected wavelength is searched for in the spectrum, and its value, in electron counts, identified. This is then multiplied by the contrast fraction factor, and the resulting final electron count value is added to the appropriate oversampled detector pixel in the generated array. For the configurations using NIRSpec's gratings, the script also takes into account order -2. If a wavelength, λ , of order -1 is incident on a

detector pixel, then $\lambda/2$ of order -2 also falls on the same pixel. Accordingly, the script takes the corresponding electron count value from the pre-generated order -2 SED and, applying the same logic to it as for the order -1 light, adds its final contrast-adjusted electron count value to the oversampled detector array.

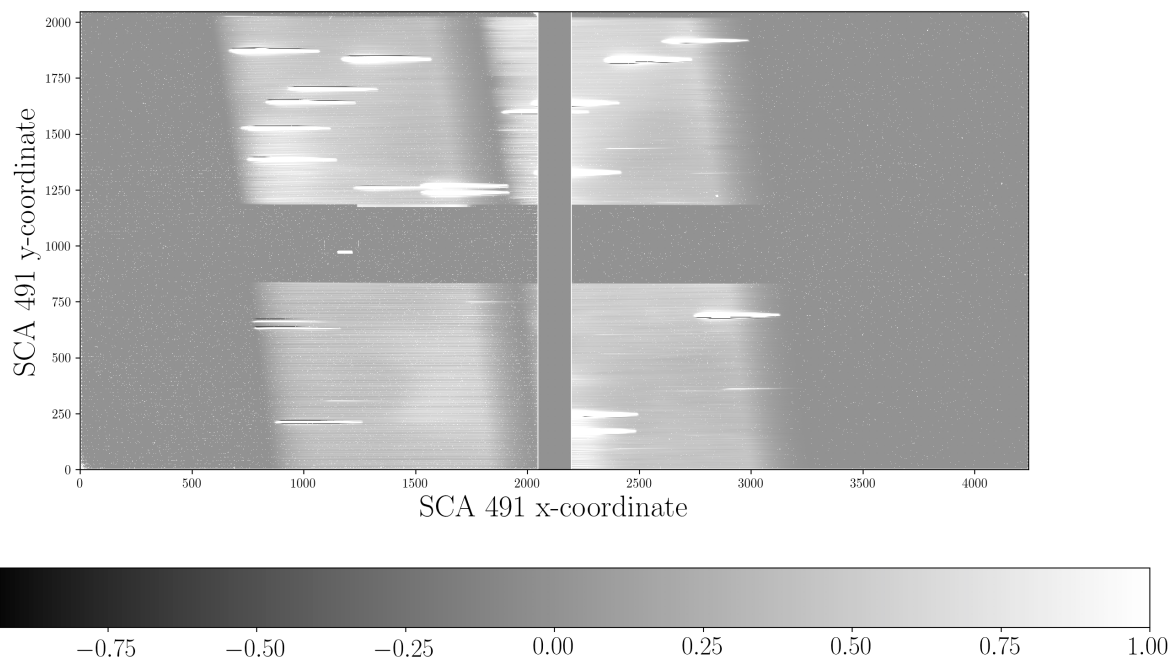
Finally, `L_model.py` also simulates the zeroth order imprint that is seen in the cases of the medium resolution gratings. It accomplishes this using the same technique that is used to model the leakage in imaging mode. It iterates through each high-resolution pixel of each shutter, then scales its value using the corresponding factor, and identifies the oversampled detector pixel corresponding to it. Then, for each oversampled detector pixel, all identified and scaled high-resolution points are integrated over. The end result is a simulated and oversampled detector image of the dispersed MSA leakage.

4 TESTING THE SPECTRAL MODEL

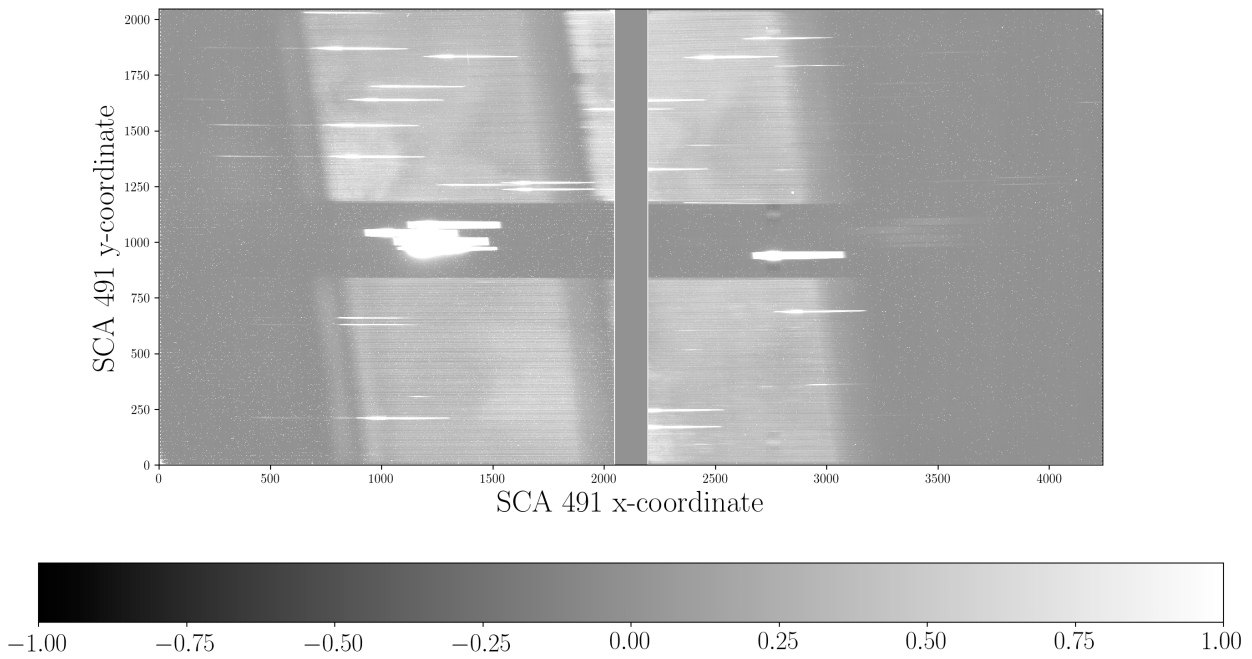
4.1 The Prism

We first simulated the MSA leakage for the prism configuration, in the case that the illumination is being provided by the internal CAA FLAT5 lamp. Here, the spectrum of the lamp was defined by the file `CAA03_CS5.fits`. An oversampling by 20 in the spatial direction was chosen. The resulting modeled exposure, together with the residuals of subtracting the model from a comparable, actual exposure of the leakage are shown in Figure 9. From these, it appears the model accurately places the leakage on the detector.

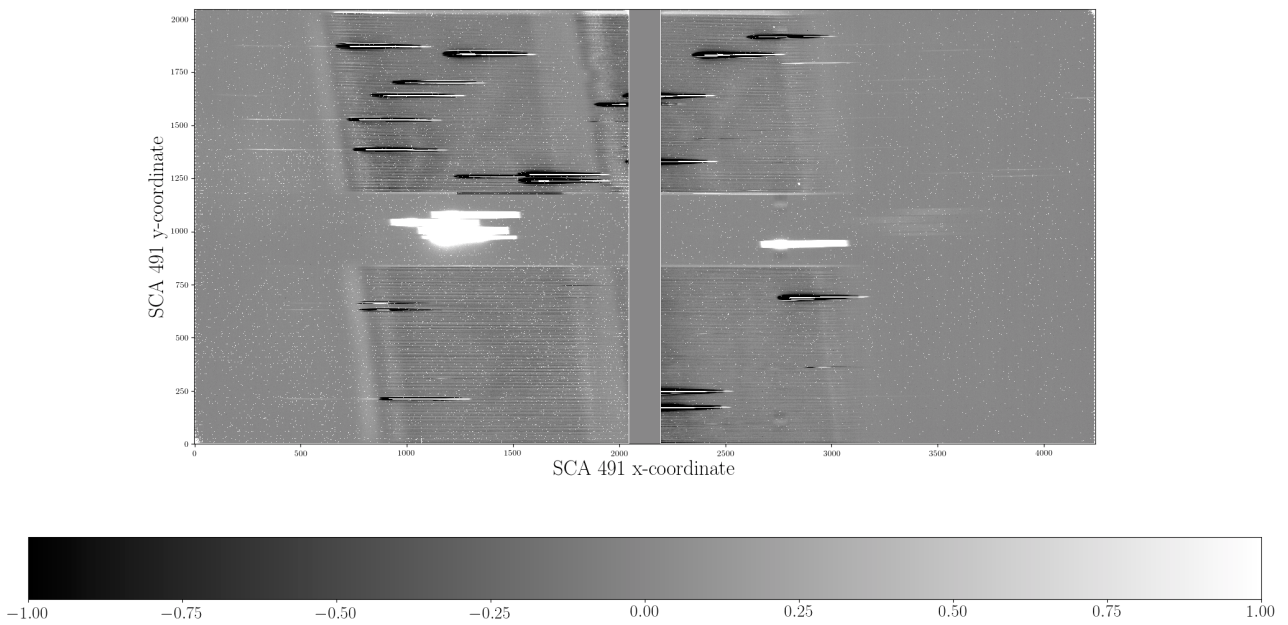
However, Figure 9d, reveals that the model’s accuracy in estimating the magnitude of the leakage, can vary significantly across the detector. The distributions of signal before and after subtraction of the model are given in Figure 10. Figure 11 elucidates the details of the variation, by showing how the model of the leakage compares to the measured leakage at four different sections of the detector. In Figure 9d, we see faint structure that matches the residuals from Figures 4b and 5. Specifically, despite the correction applied to the model using the imaging residuals, the heightened levels of over-subtraction in these regions persist. This effect is responsible for the largest discrepancies between the model and the data.



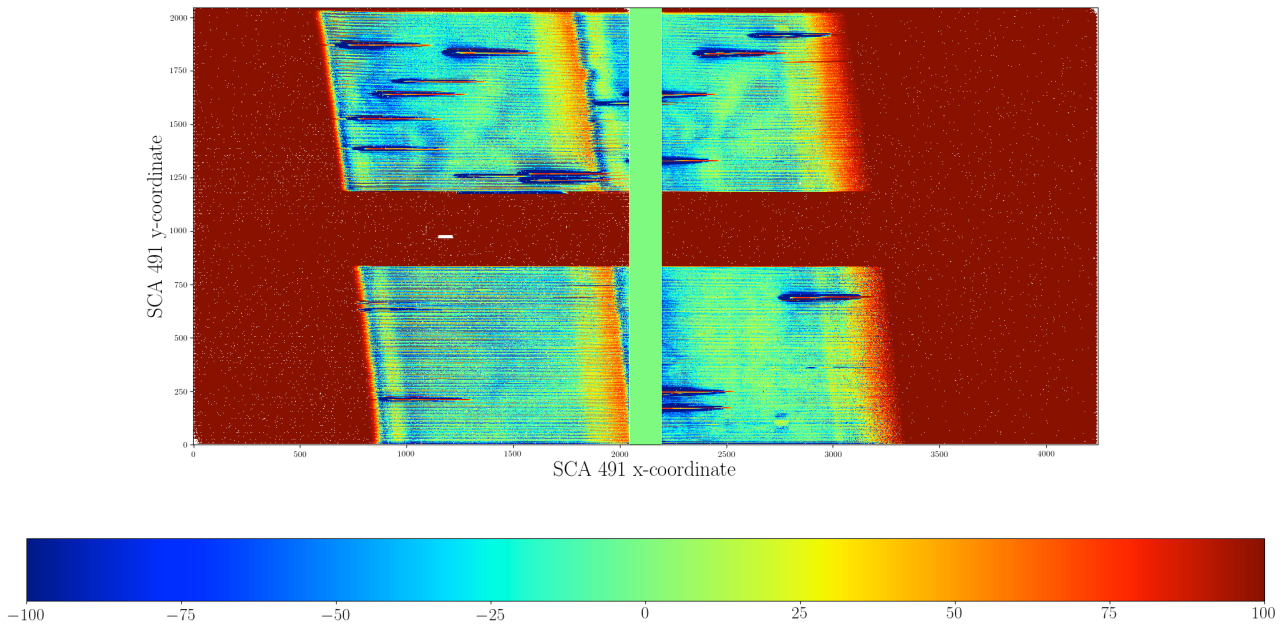
(a) Simulated exposure of spectral MSA leakage for CAA lamp FLAT5, with the prism. Values are in electron counts.



(b) Exposure NID 30362 obtained with CAA lamp FLAT5.



(c) Residuals of subtracting Figure 9a, from a corresponding, actual exposure. Values in electron counts.



(d) Residuals of the same subtraction as in Figure 9c, however, as a percentage of the measured leakage signal.

Figure 9: Model of dispersed MSA leakage for the prism configuration when illuminated by internal CAA lamp FLAT5, together with the residuals of its subtraction from exposure NID 30362. This exposure was also obtained by using CAA FLAT5 on NIRSpec’s prism.

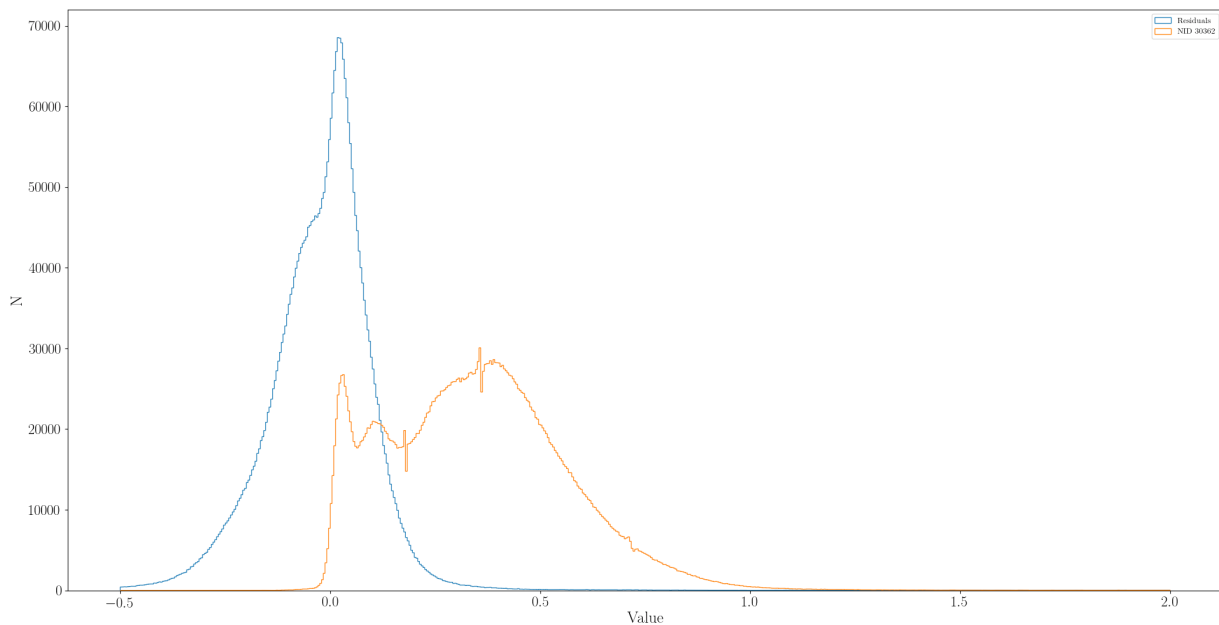
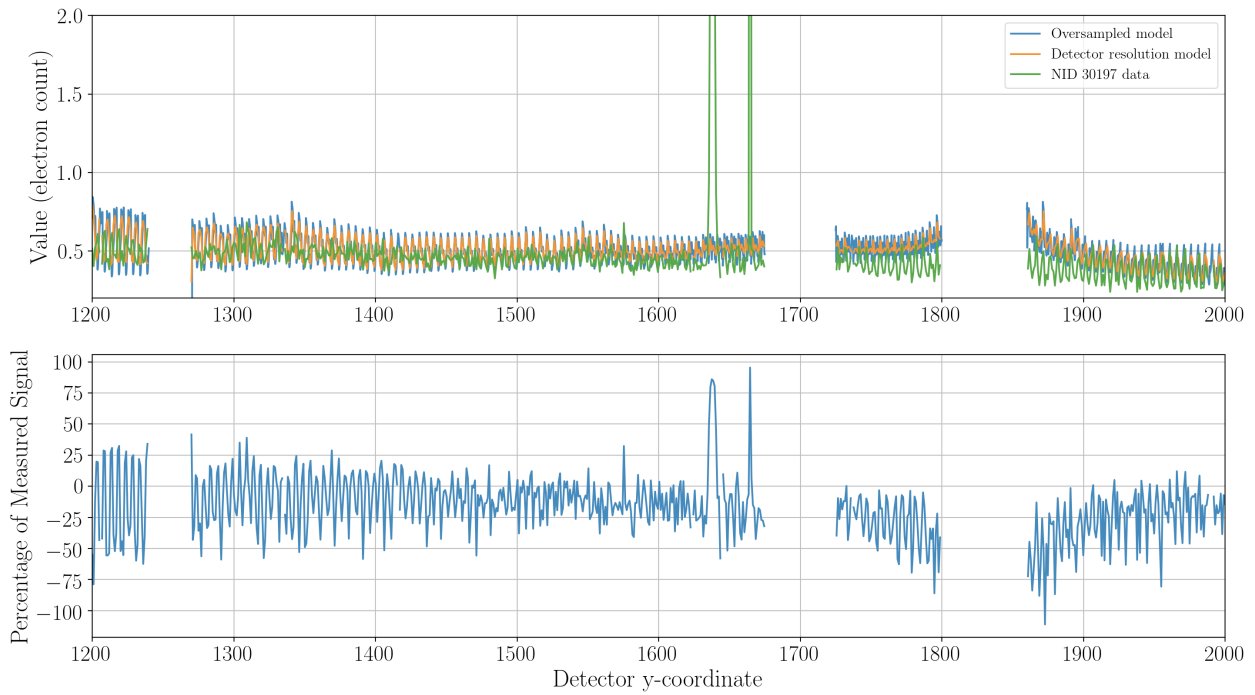
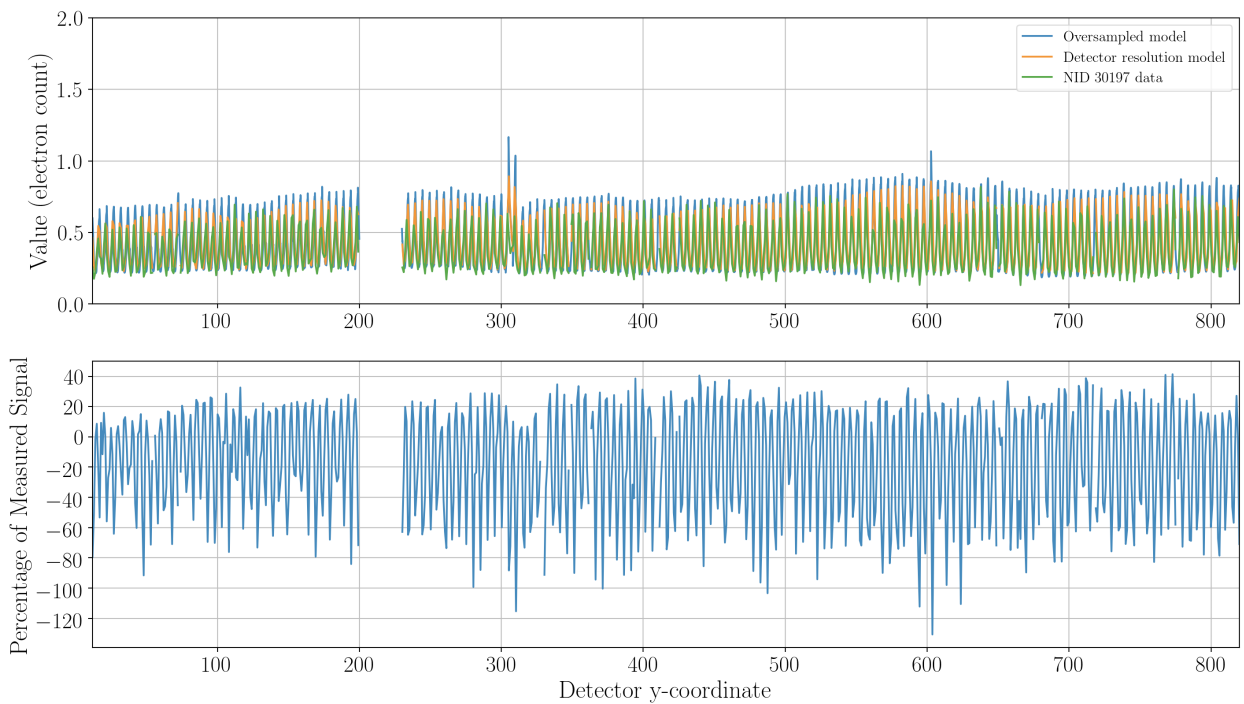


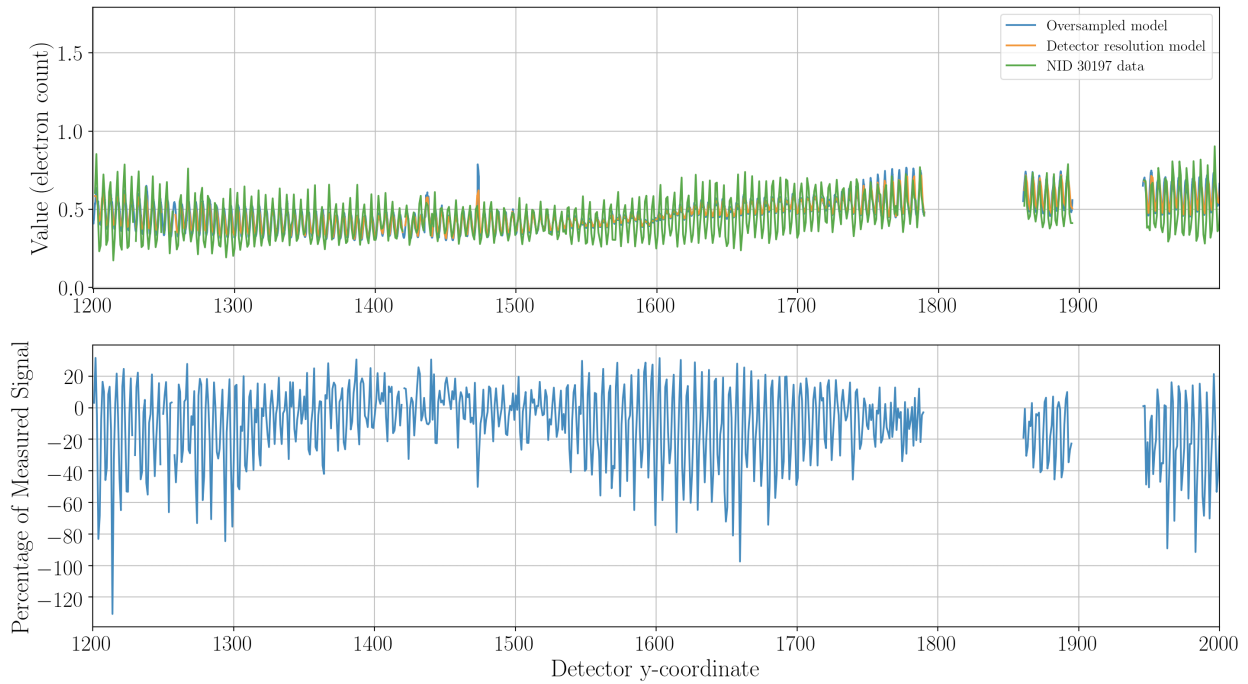
Figure 10: Histograms showing distribution of values in NID 30362, and the residuals of subtracting a corresponding simulated exposure from this.



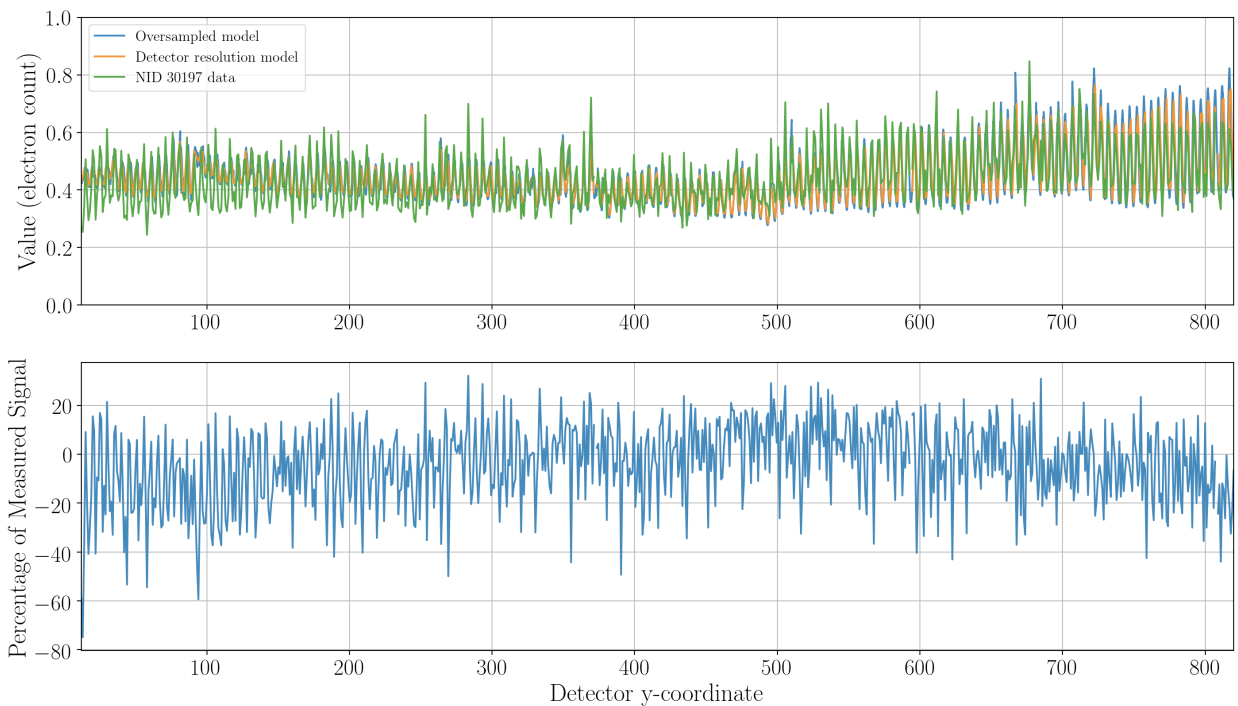
(a) Extract between SCA491 y-coordinates 1200 - 2000, at SCA491 x-coordinate 1250.



(b) Extract between SCA491 y-coordinates 12 - 820, at SCA491 x-coordinate 1250.



(c) Extract between SCA491 y-coordinates 1200 - 2000, at SCA491 x-coordinate 2625.



(d) Extract between SCA491 y-coordinates 12 - 820, at SCA491 x-coordinate 2625.

Figure 11: Comparison of model values and measured values in NID 30398, together with residuals of subtracting modeled values from measured values, as percentage of measured values. Regions with FO shutters or poor quality flags have been masked.

In addition, towards the right-handed edges of each quadrant in Figure 4b, we see a sudden increase in the residuals as a percentage of measured leakage signal. This is mainly due to the fact that the leakage spectra themselves drops of significantly in these regions meaning that, even though it is clear from Figure 9c the magnitude of the residuals here is low, relative to the now low leakage signal it appears to be higher.

Furthermore, Figure 11 reveals a more subtle pattern of oscillating over-subtraction and under-subtraction which matches the oscillation between higher and lower levels of leakage, that occurs across the detector. In general, we find that when the levels of leakage peak, there is under-subtraction, typically confined within $\sim < 25\%$. Conversely, when the leakage is at a trough, the model over-subtracts. This over-subtraction effect is less well constrained than the under-subtraction, with the levels of residuals regularly reaching, and at times exceeding, 60%. This is also reflected in Figure 10, where the histogram of residuals is not completely symmetric around zero, having a higher negative side. This effect is best demonstrated by and most pronounced in the case of MSA quadrant 4, as can be seen in Figures 9d and 11b. In Figure 4b, we see that Q4 uniquely does not possess any low-contrast, over-subtracted regions. Therefore, the over-subtraction found in the dispersed Q4 is owed exclusively to the oscillation effect. In addition, over-subtraction part of this effect is particularly egregious here, owing to the structure of the leakage in this quadrant's shutters.

Given that most of the leakage is concentrated in the shutter bars, there are large regions with low levels of leakage; leading to large regions of over-subtraction in the dispersed model. It is speculated that this effect is the result of using a single coefficient per shutter, when scaling the high-resolution shutter maps. A single scale factor likely does not fully capture the distribution of leakage across a micro-shutter; instead underestimating regions that should be higher, whilst over-estimating regions that should be lower.

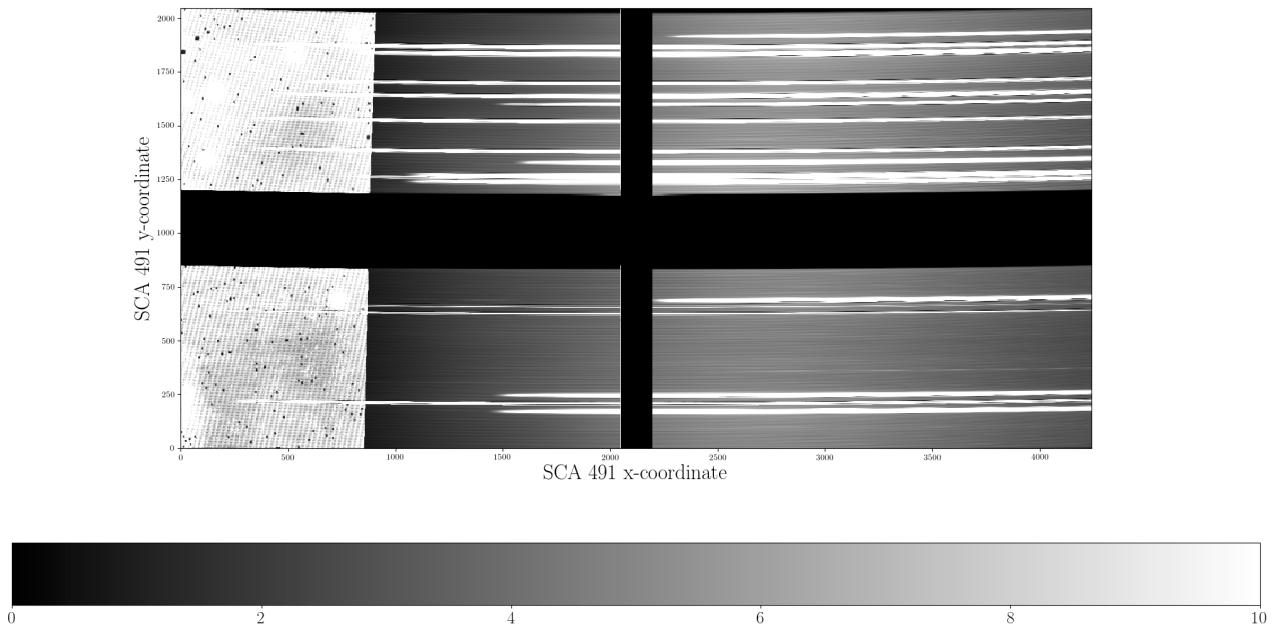
4.2 G140M

Next, we simulated a calibration exposure for the grating G140M; illuminated by CAA FLAT1. This lamp is equivalent to an extended external source viewed through the filter F100LP. The spectrum was encapsulated in CAA03_CS1.fits, and an oversampling factor of 10 was employed. In addition to the spectral MSA leakage, this exposure also contains an imprint of the zeroth order of the leakage. The simulation is shown in Figure 12a. Residuals of subtracting this from a comparable testing exposure are given in Figure 12b.

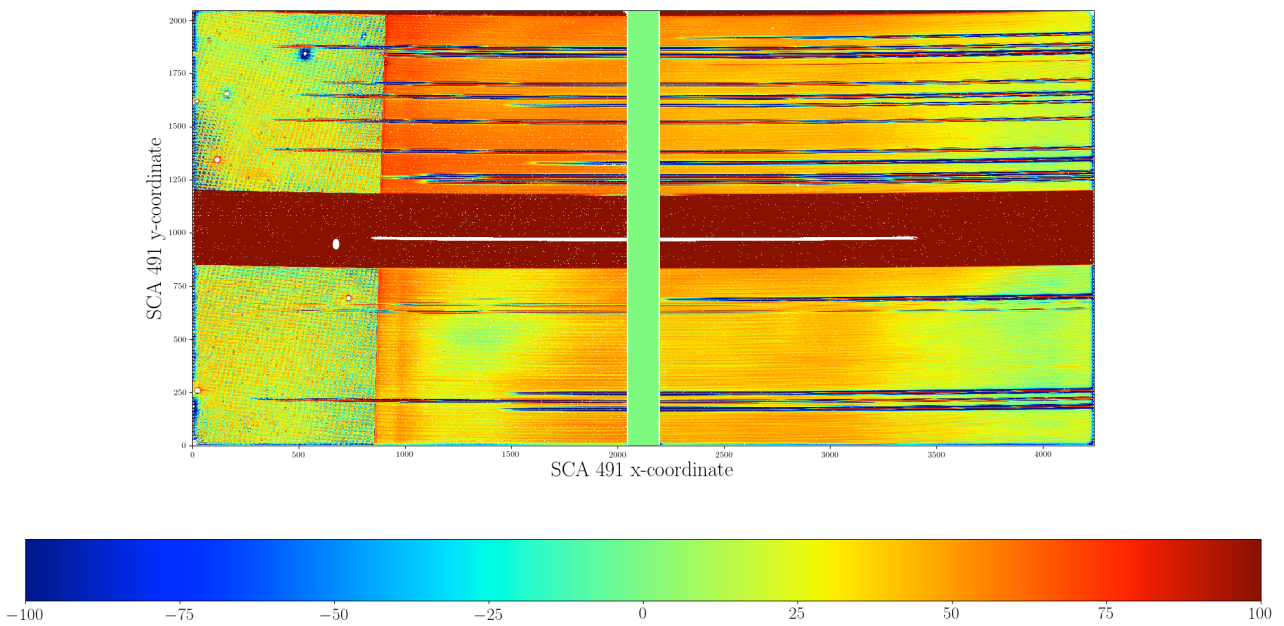
Once more, the model seems to correctly place the signal on the detector. However, examination of Figure 12b reveals a trend that runs contrary to the results from imaging and the prism. In this case, while the zeroth order imprint appears generally well subtracted, the dispersed leakage appears to be consistently under-subtracted. Interrogation of order -1 of the spectrum input into the model reveals discrepancies with the spectrum as it appears within the actual cryo-vacuum testing exposures.

In addition to suspected subtle deviations, there is a clear under-estimation of the magnitude of the spectrum. A first-order peak-to-peak comparison reveals an under-estimation by a factor of 1.62. This difference necessitates extensive further investigation, but for the purposes of this investigation, we apply a first-order correction by multiplying the spectrum by this 1.62 factor. The post-correction simulation and residuals are given below, in Figure 13. Histograms showing the effect of a model subtraction from test exposure are shown in Figure 14. As with the prism, the spatial variation of the model in comparison to the corresponding exposure at four regions on the detector is shown in Figure 15. We see in these and in Figure 13 similar trends to those observed in the case of the prism.

Once again, the accuracy of the model oscillates, with lower accuracy regions corresponding to areas where the leakage level drops. In regions of higher leakage, the model is typically within 20% of the test data, and typically within 50% for regions with low leakage. We also see similar regions of over-subtraction, following the pattern observed in imaging mode and for the prism. In addition, in Figure 15a, and in the corresponding region of Figure 13d, we see there still remains slight under-subtraction. This is likely attributable to the applied first-order correction not sufficiently compensating for the discrepancies between the input spectrum and the true spectrum.

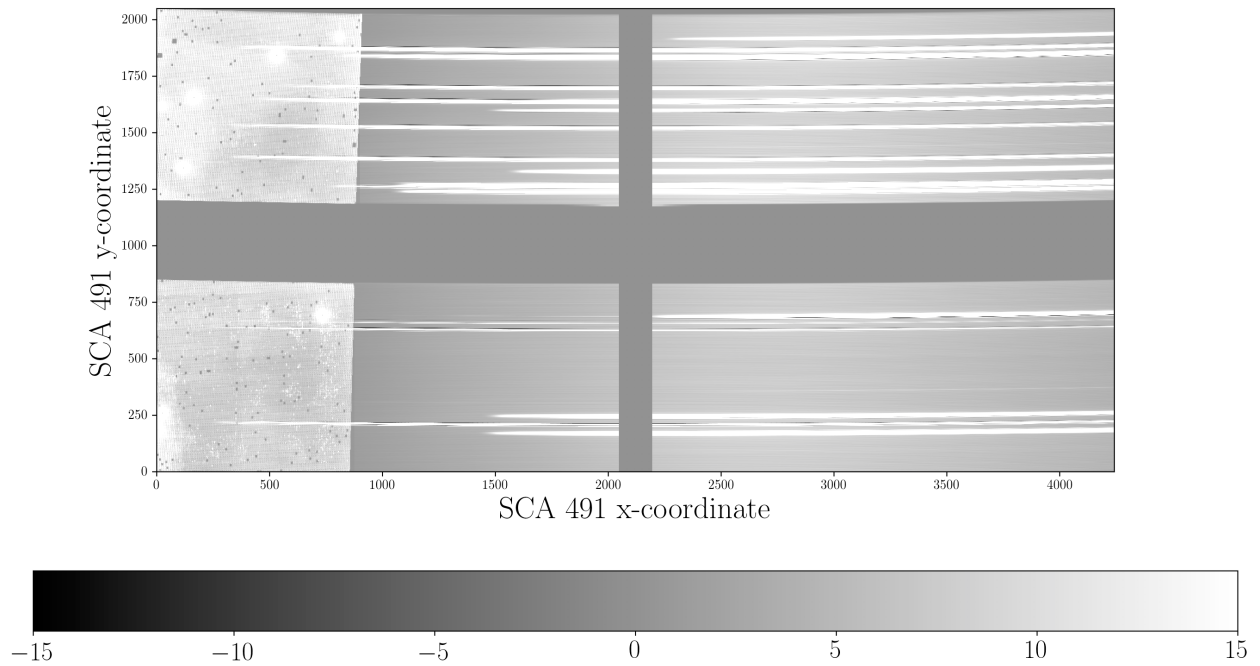


(a) Simulated exposure of spectral MSA leakage for CAA lamp FLAT1, with grating G140M. Values are in electron counts.

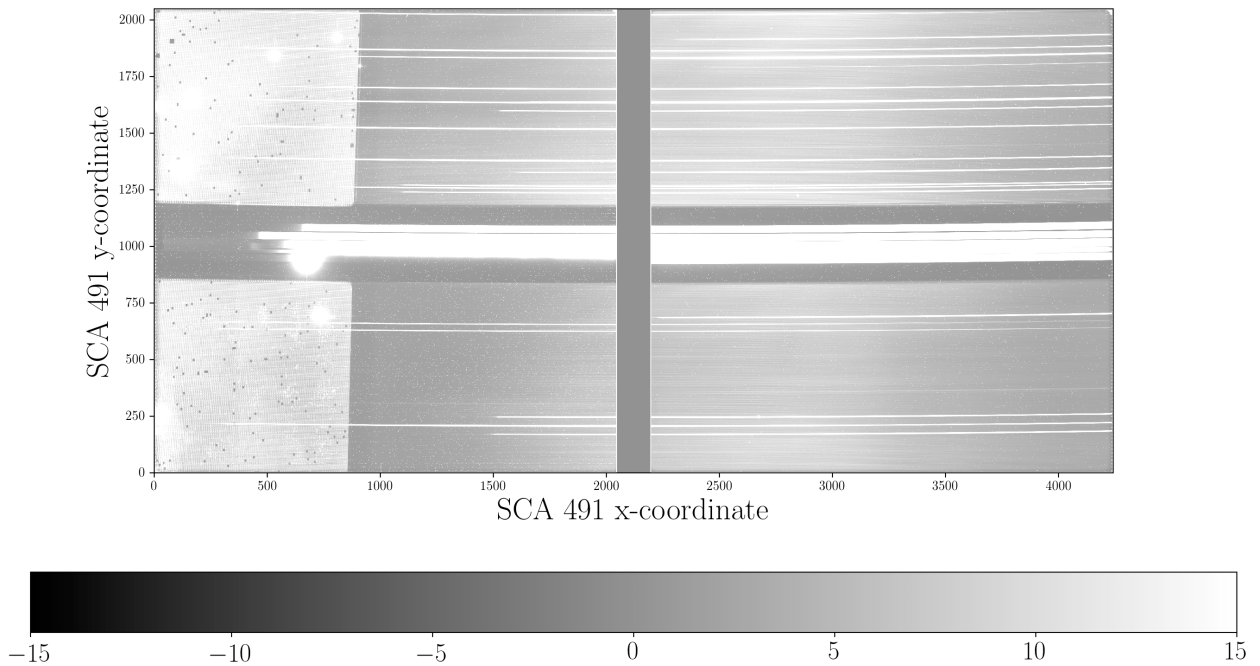


(b) Residuals of subtracting Figure 12a, from a corresponding, actual exposure as a percentage of measured leakage signal in the exposure.

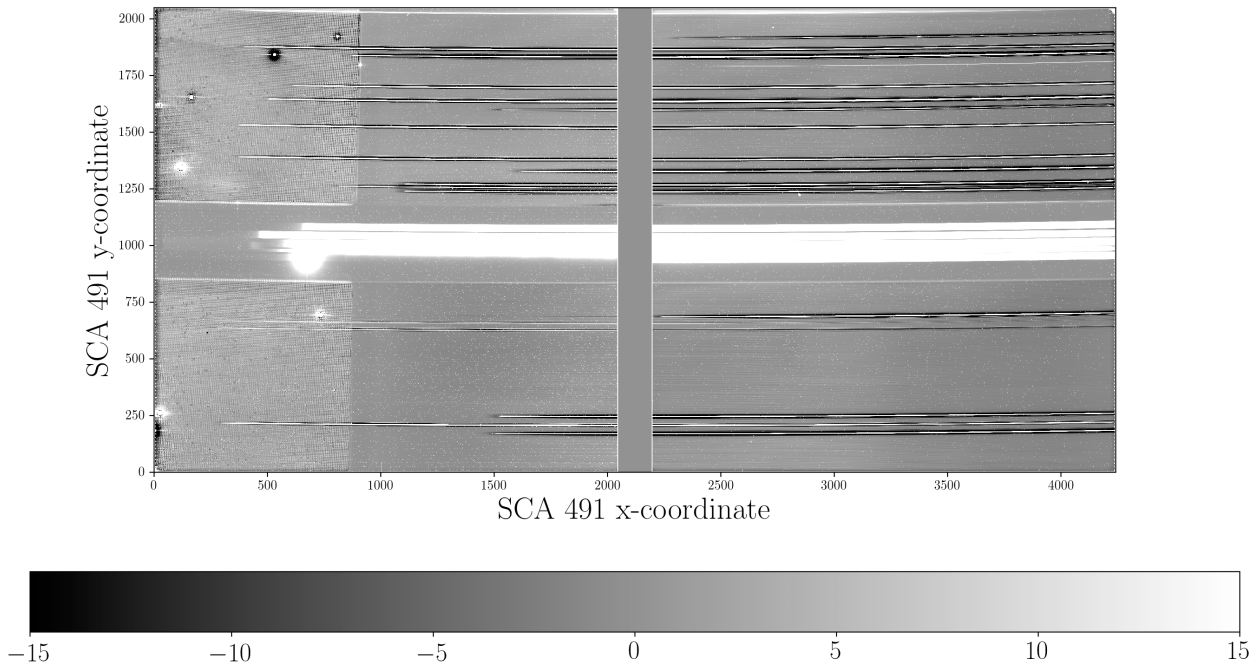
Figure 12: Model of dispersed MSA leakage for the grating G140M when illuminated by internal CAA lamp FLAT1, together with the residuals of its subtraction from exposure NID 30197, also obtained by using CAA FLAT1 on G140M.



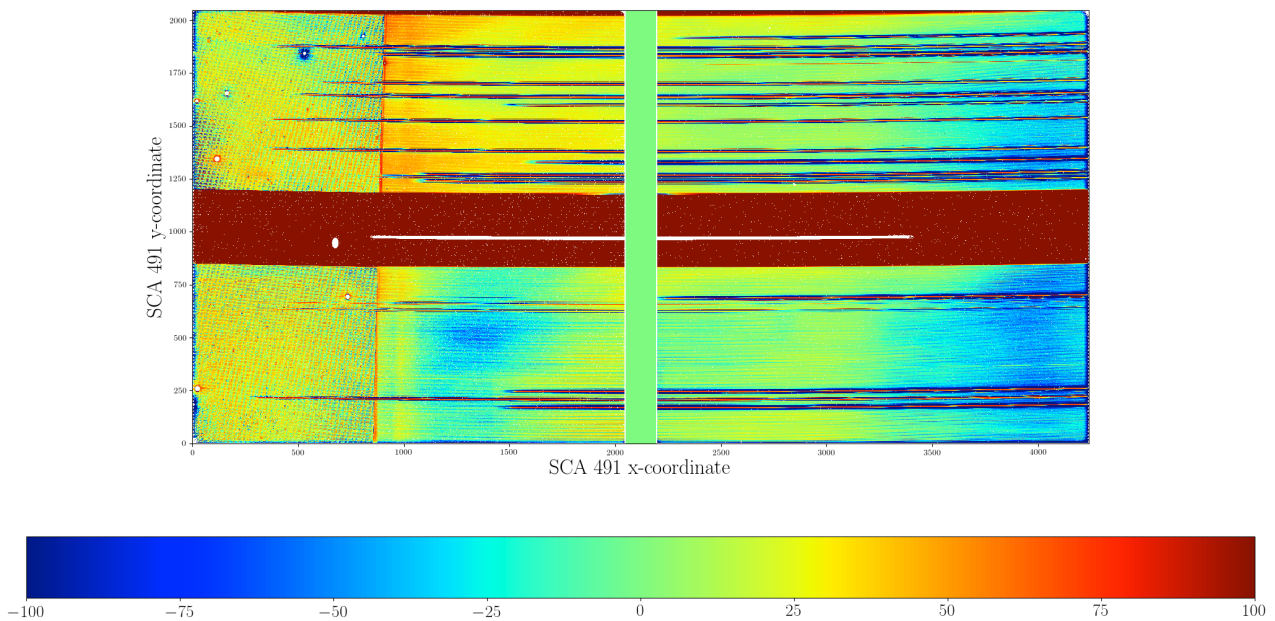
(a) Simulated exposure of spectral MSA leakage for CAA lamp FLAT1 using grating G140M, with first-order correction. Values are in electron counts.



(b) Residuals of subtracting Figure 13a, from a corresponding, actual exposure. Values in electron counts.



(c) Exposure NID 30197 obtained with CAA lamp FLAT1.



(d) Residuals of subtracting Figure 13a, from a corresponding, actual exposure as a percentage of measured leakage signal in the exposure.

Figure 13: Corrected model of dispersed MSA leakage for the grating G140M when illuminated by internal CAA lamp FLAT1, together with the residuals of its subtraction from exposure NID 30197. This exposure was also obtained by using CAA FLAT1 on G140M.

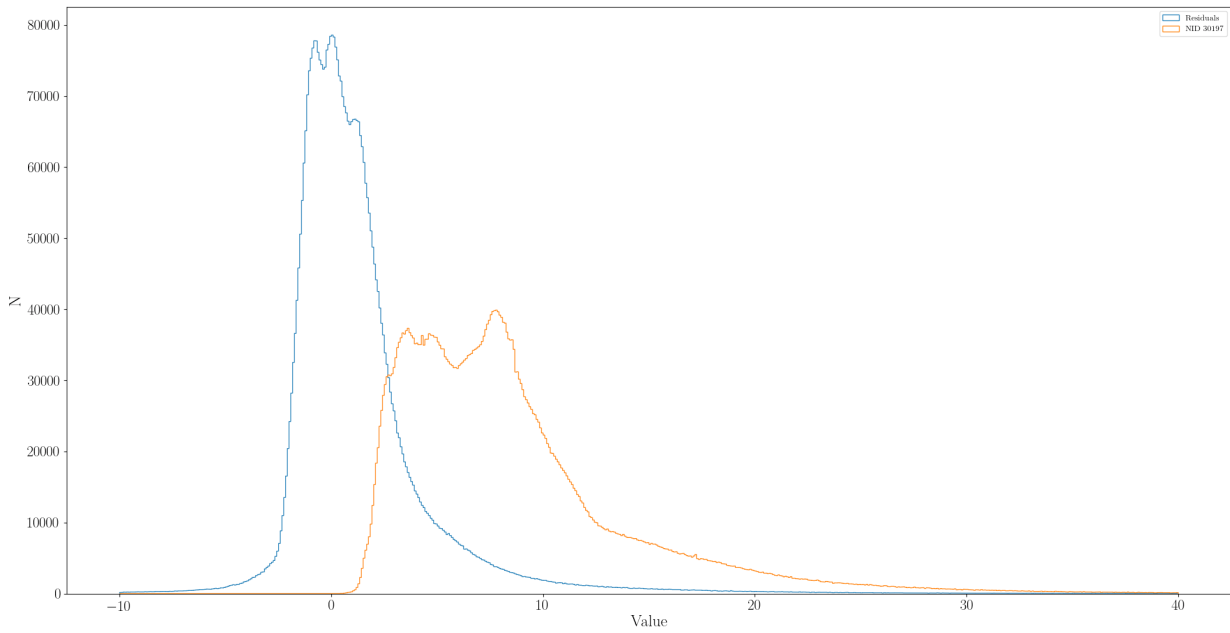
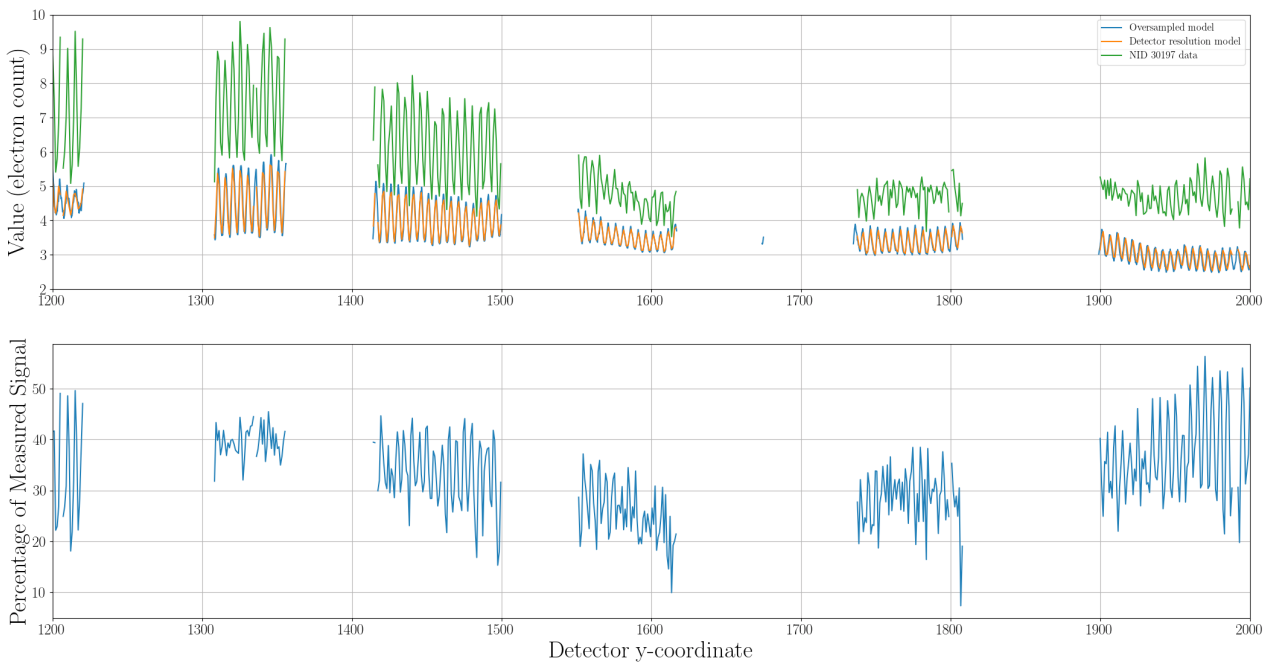
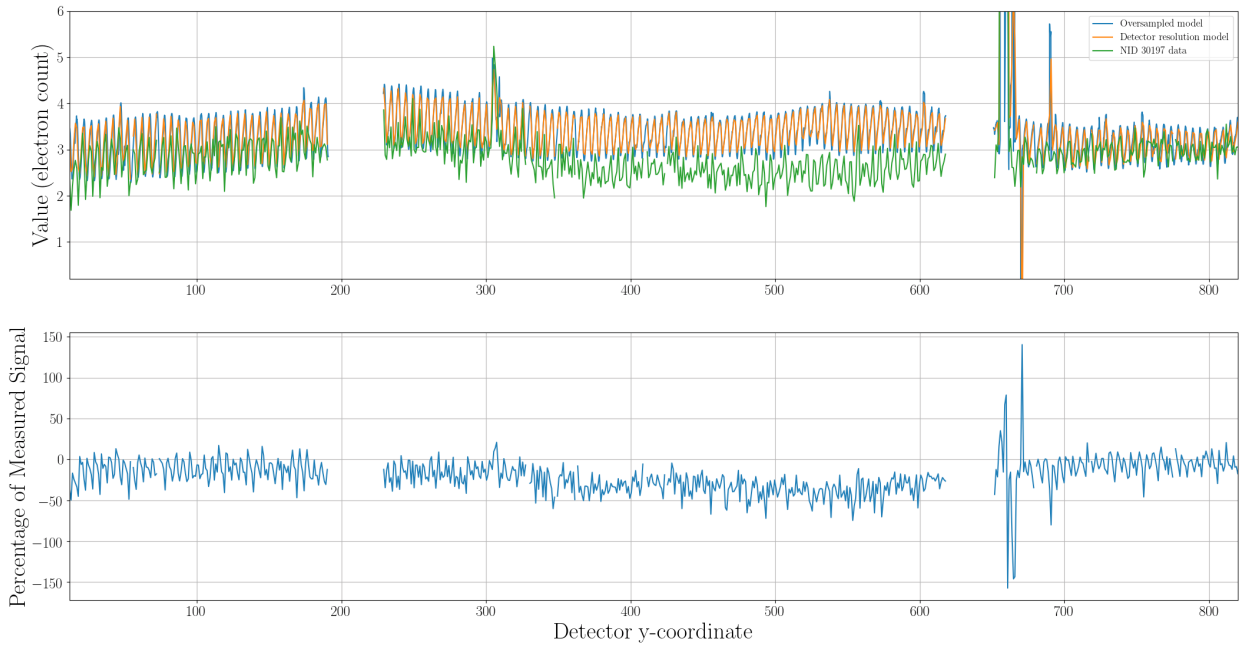


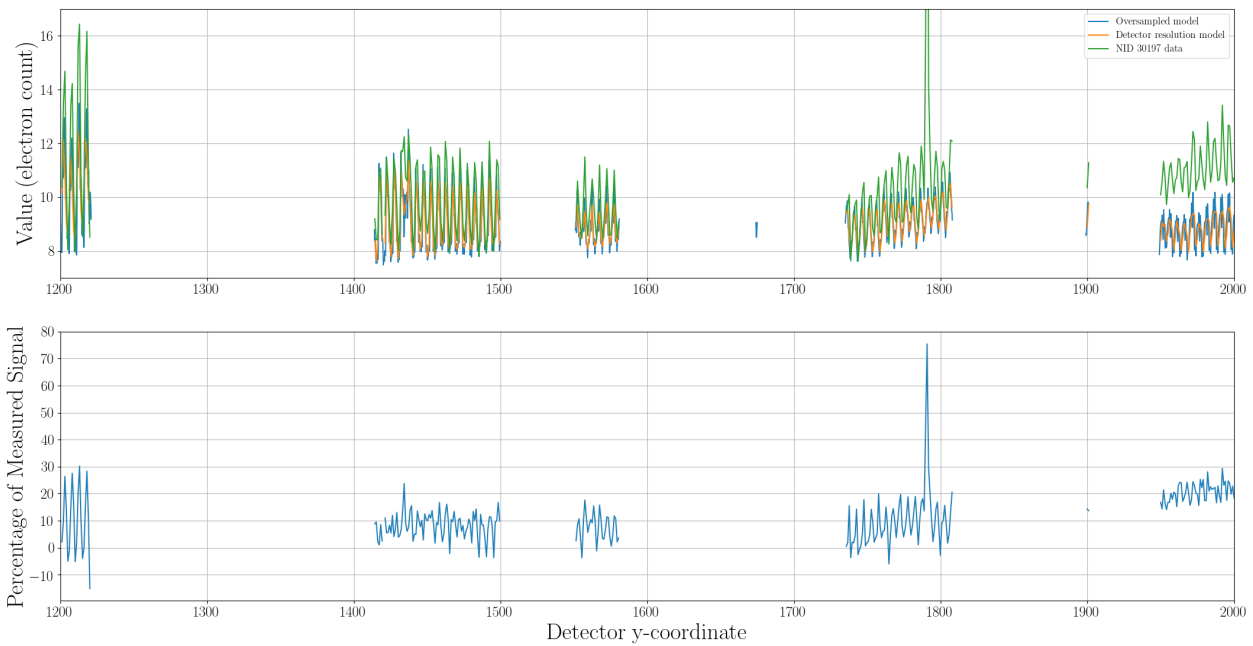
Figure 14: Histograms showing distribution of values in NID 30197, and the residuals of subtracting a corresponding corrected simulated exposure from this.



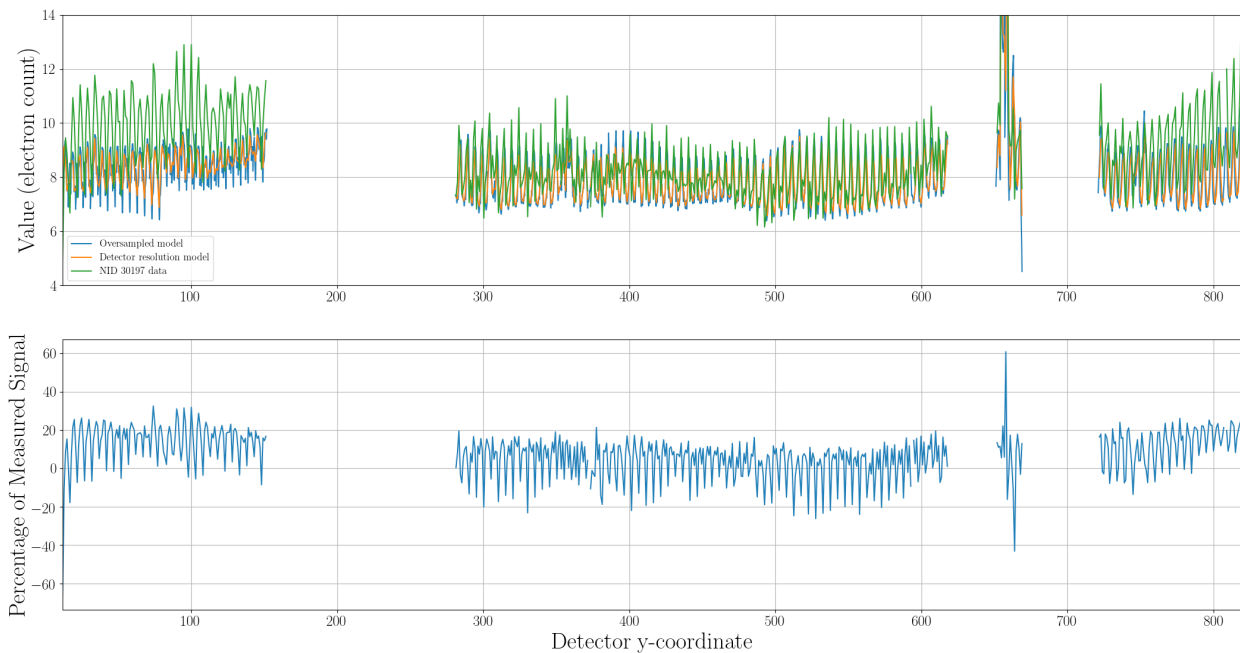
(a) Extract between SCA491 y-coordinates 1200 - 2000, at SCA491 x-coordinate 1250.



(b) Extract between SCA491 y-coordinates 12 - 820, at SCA491 x-coordinate 1250.



(c) Extract between SCA491 y-coordinates 1200 - 2000, at SCA491 x-coordinate 2625.



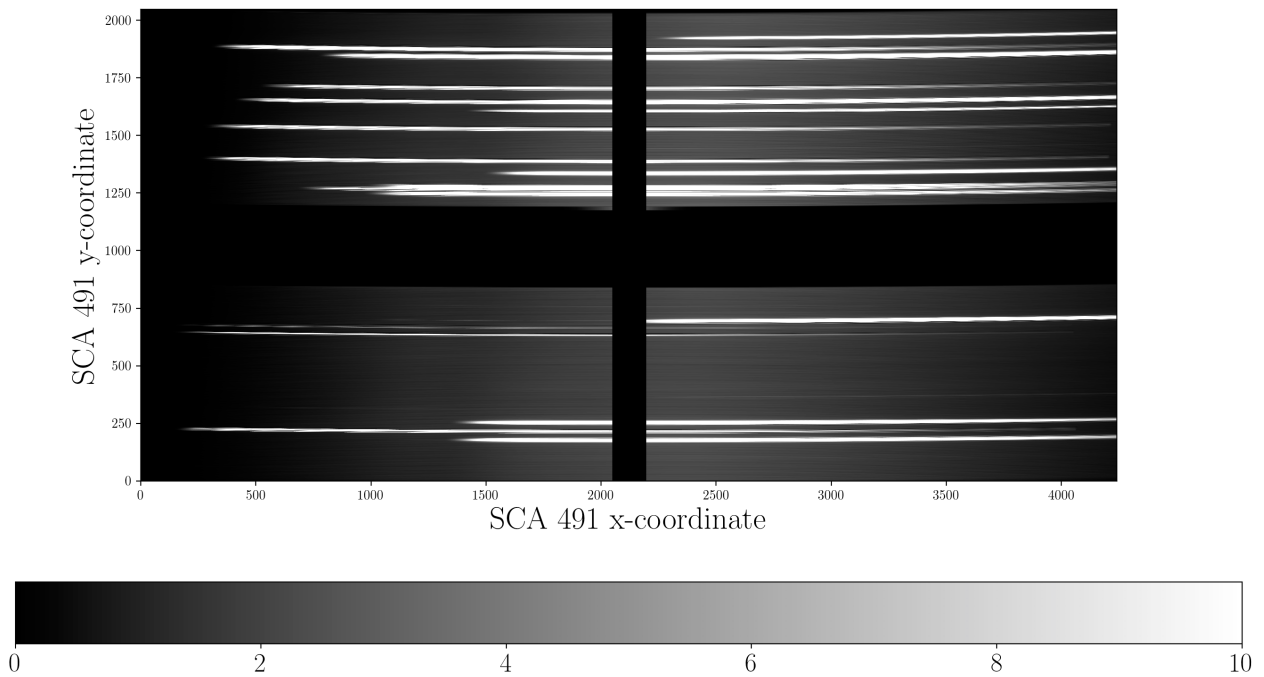
(d) Extract between SCA491 y-coordinates 12 - 820, at SCA491 x-coordinate 2625.

Figure 15: Comparison of model values and measured values in NID 30197, together with residuals of subtracting modeled values from measured values, as percentage of measured values. Regions with FO shutters or poor quality flags have been masked.

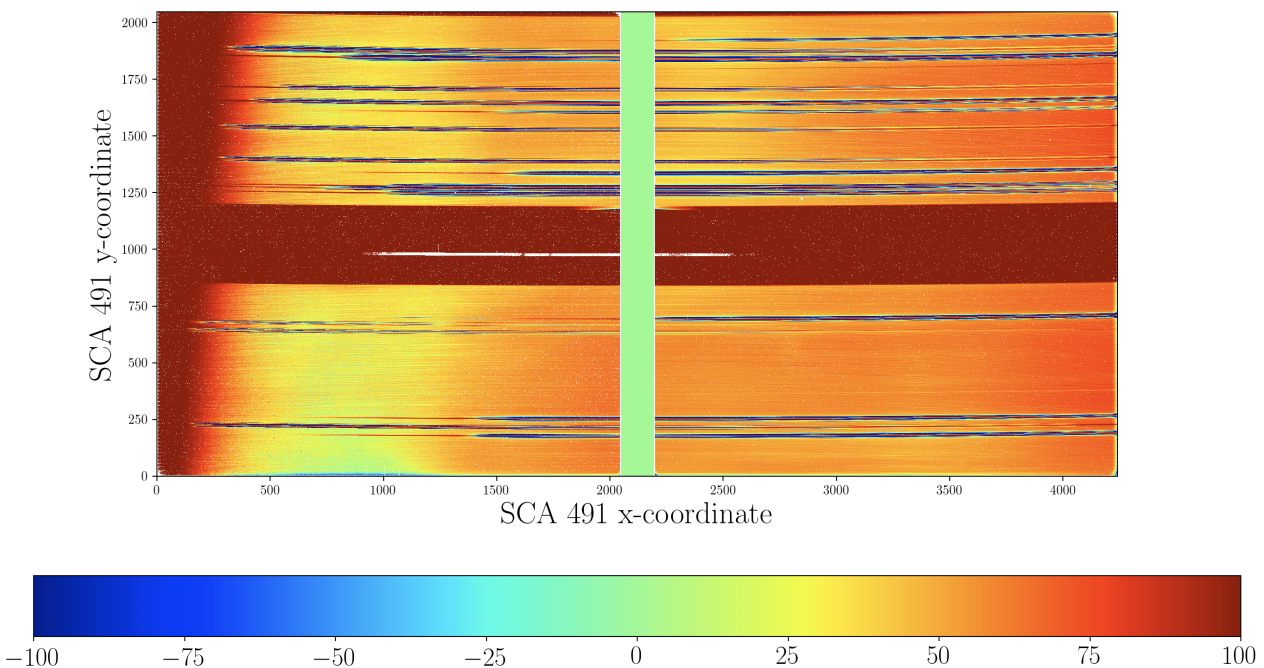
4.3 G395H

In order to check how the model deals with the high-resolution gratings, we also simulated an exposure of the grating G395H being illuminated by CAA FLAT3. This lamp is equivalent to an extended external source viewed through the filter F290LP. For modelling purposes, the lamp's spectrum was defined by the file `CAA03_CS3.fits`. As with the G140M simulations, an oversampling factor of 10 was applied in the spatial direction. The simulated exposure is shown in Figure 16a, while the relative residuals of subtracting these from a comparable cryo-vacuum ground testing exposure are given in Figure 16b. We see from the residuals that, yet again, the model's placement of leakage on the detector is correct. However, as was the case for G140M, there is a clear trend of under-subtraction across the detector. Examination of the input spectrum used in the model reveals that, as was the case for G140M, the intensity is lower than what is seen from testing exposures. The peak of the input spectrum was found to be a factor of 1.64 lower than the peak of the measured spectrum. This factor was applied as a first order correction, in order to produce an updated simulation. This together with its own residuals is shown in Figure 17. Histograms showing the effect of subtracting this simulation from an equivalent testing exposure are given in Figure 18. The spatial variation of the model in comparison to the corresponding exposure at four regions on the detector is shown in Figure 19.

The updated simulation is consistent with the case of imaging, and the case of the prism. Across Figure 19, we once again see the familiar pattern of oscillating over-subtraction and under-subtraction. In Figure 17, we also see the over-subtracted imprint of the poorly modelled low-contrast shutters, as would be expected. In keeping with the previous configurations, in regions of higher leakage the model is typically within 20% of the test data, and 50% for regions with low leakage. Additionally, the model generally under-subtracts at higher wavelengths. This systematic under-subtraction can also be seen as the second peak in Figure 18. This is expected, and consistent with the results of 1D modelling (Deshpande 2017). It is a consequence of the input spectrum used poorly modelling the true CAA FLAT3 spectrum at its higher wavelength tail. To gain a holistic understanding of the model's accuracy, it is necessary to probe the discrepancies between spectra deeper.

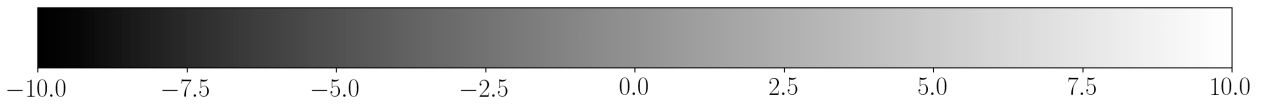
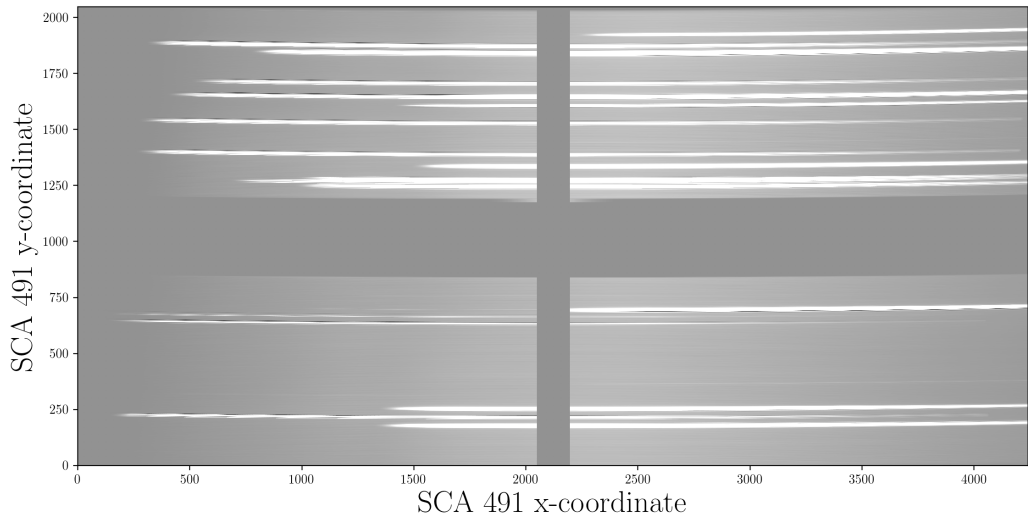


(a) Simulated exposure of spectral MSA leakage for CAA lamp FLAT3, with grating G395H. Values are in electron counts.

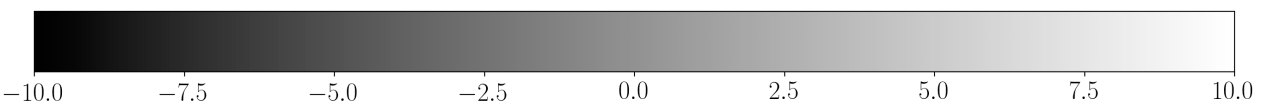
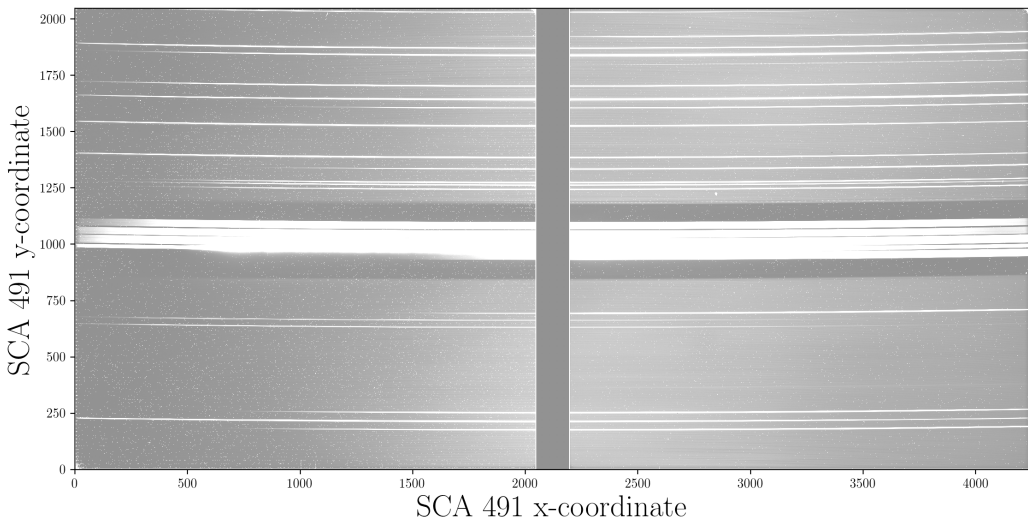


(b) Residuals of subtracting Figure 16a, from a corresponding, actual exposure as a percentage of measured leakage signal in the exposure.

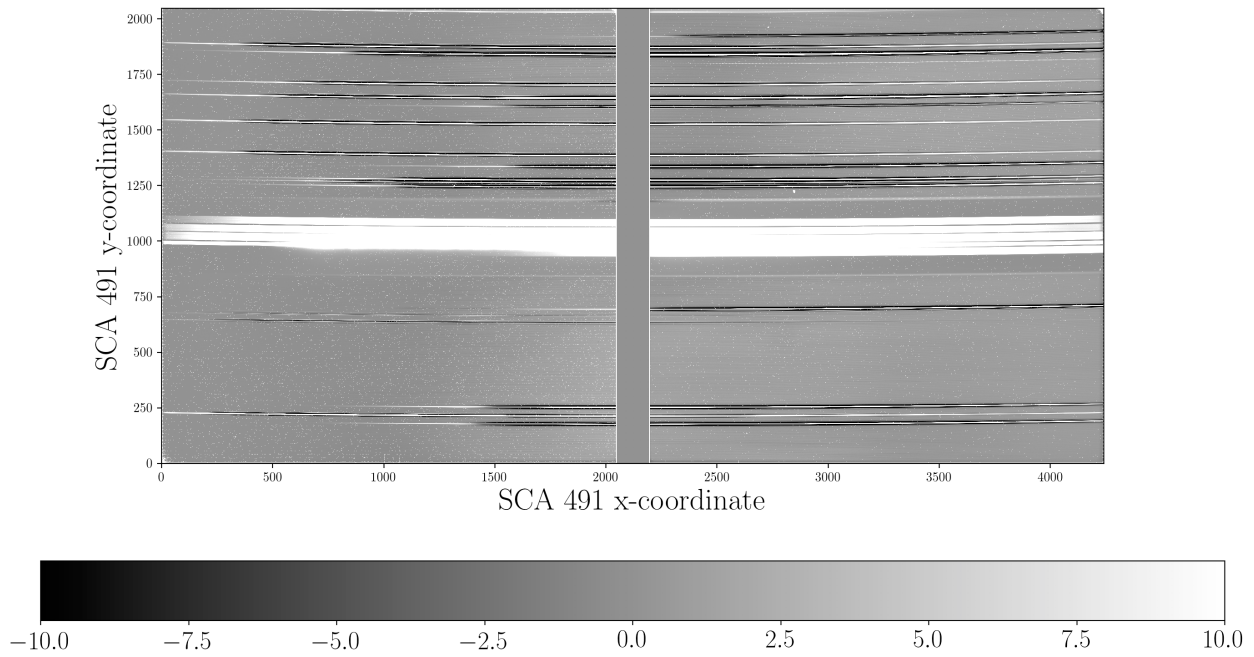
Figure 16: Model of dispersed MSA leakage for the grating G395H when illuminated by internal CAA lamp FLAT3, together with the residuals of its subtraction from exposure NID 30161, also obtained by using CAA FLAT3 on G395H.



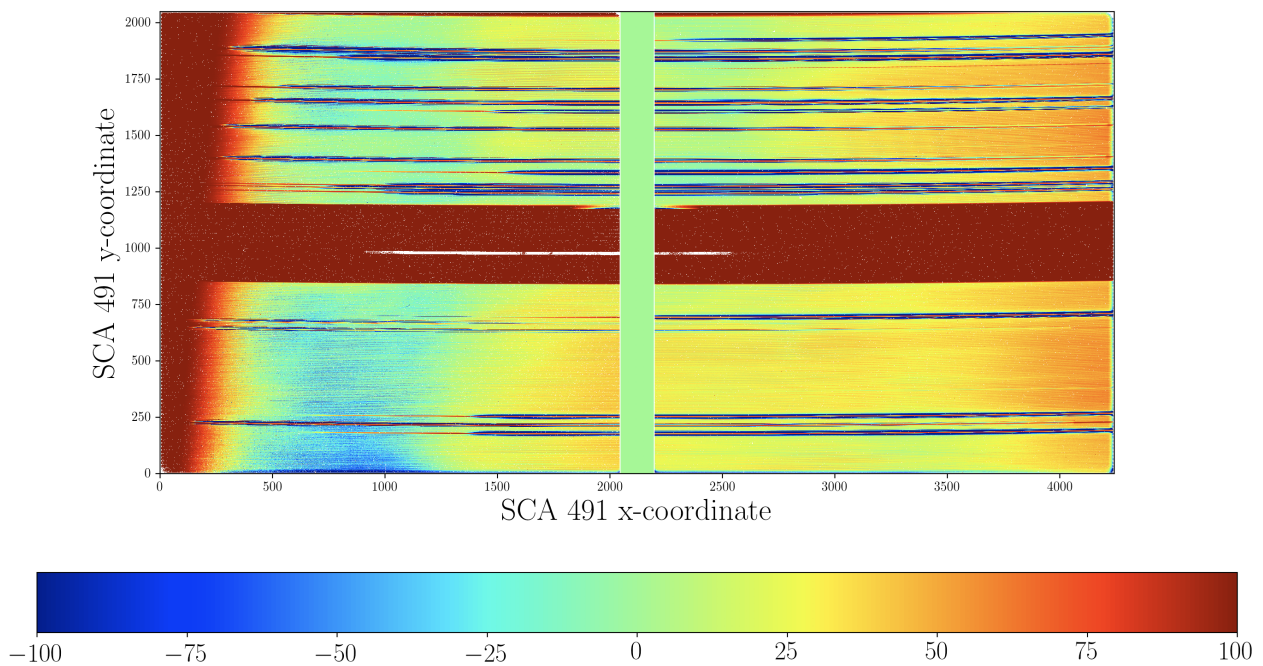
(a) Simulated exposure of spectral MSA leakage for CAA lamp FLAT3 using grating G395H, with first-order correction. Values are in electron counts.



(b) Exposure NID 30161 obtained with CAA lamp FLAT3.



(c) Residuals of subtracting Figure 17a, from a corresponding, actual exposure. Values in electron counts.



(d) Residuals of subtracting Figure 17a, from a corresponding, actual exposure as a percentage of measured leakage signal in the exposure.

Figure 17: Corrected model of dispersed MSA leakage for the grating G140M when illuminated by internal CAA lamp FLAT3, together with the residuals of its subtraction from exposure NID 30161. This exposure was also obtained by using CAA FLAT3 on G395H.

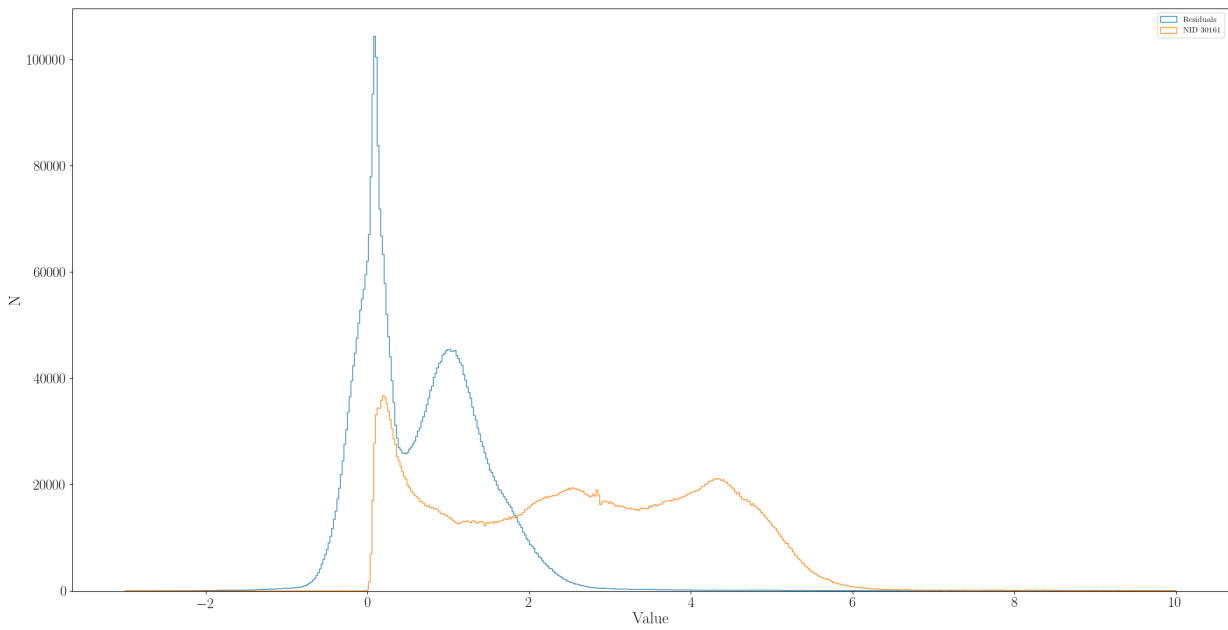
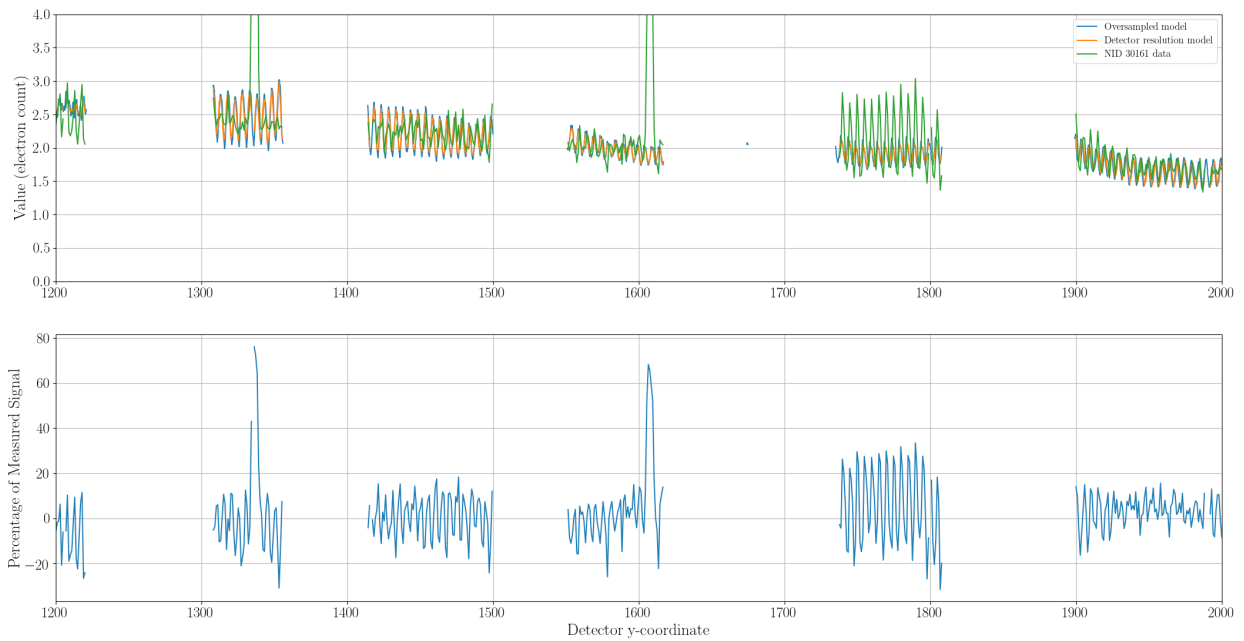
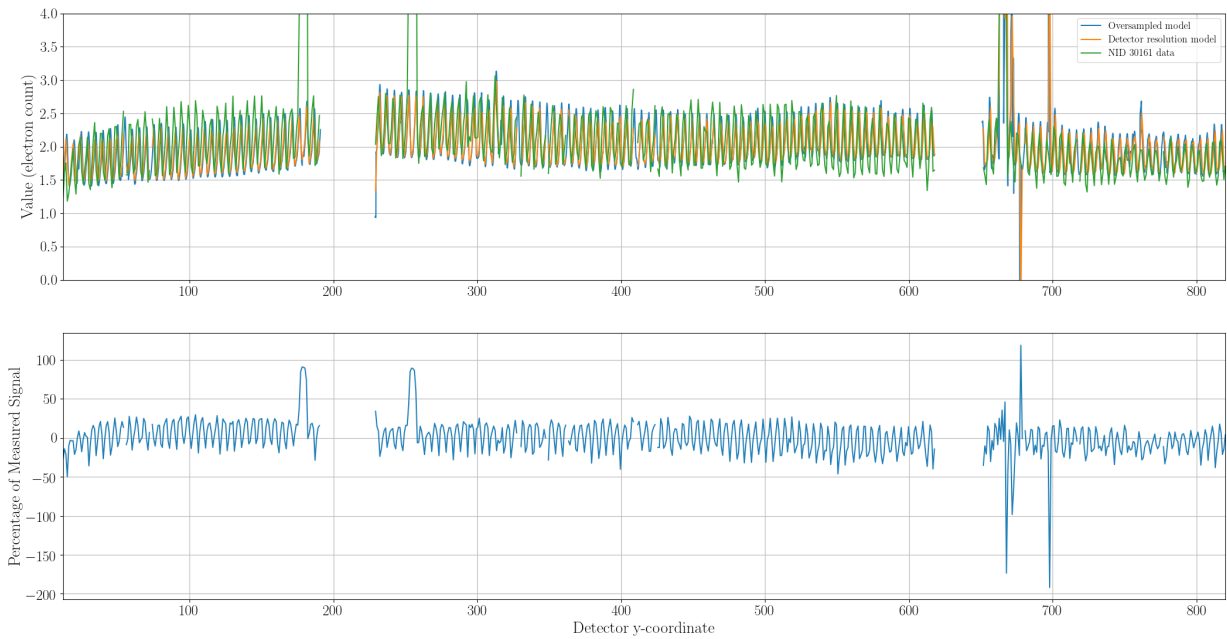


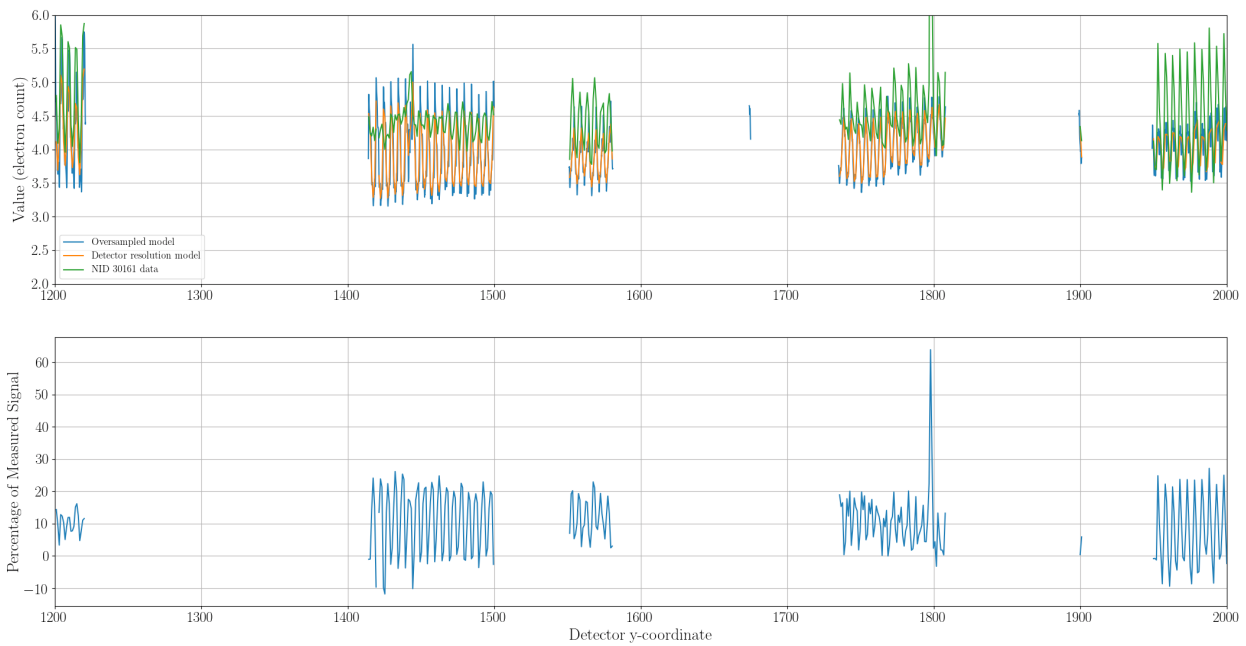
Figure 18: Histograms showing distribution of values in NID 30161, and the residuals of subtracting a corresponding corrected simulated exposure from this.



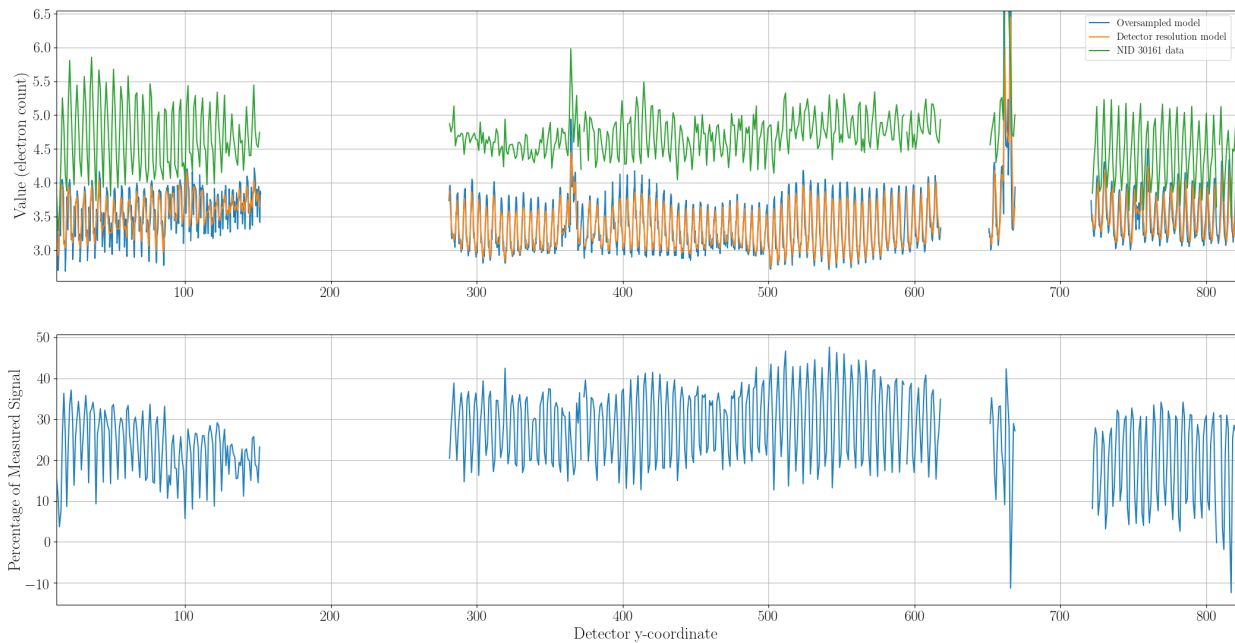
(a) Extract between SCA491 y-coordinates 1200 - 2000, at SCA491 x-coordinate 1250.



(b) Extract between SCA491 y-coordinates 12 - 820, at SCA491 x-coordinate 1250.



(c) Extract between SCA491 y-coordinates 1200 - 2000, at SCA491 x-coordinate 2625.



(d) Extract between SCA491 y-coordinates 12 - 820, at SCA491 x-coordinate 2625.

Figure 19: Comparison of model values and measured values in NID 30161, together with residuals of subtracting modeled values from measured values, as percentage of measured values. Regions with FO shutters or poor quality flags have been masked, however, some unmasked bad data still remains.

5 CONCLUSION

A comprehensive analysis of the spurious parasitic signal known as ‘MSA Leakage’ revealed the need for a detailed, 2D, spectral model of this signal. In view of better characterisation of this signal, and potential use in mitigation strategies, this investigation set out to construct such a spectral model. The complexities of this signal, such as variation due to repositioning of NIRSpec’s grating wheel, meant that a high-resolution model was necessary. This high-resolution requirement generated the additional challenge of computational efficiency.

Building on previous work, we constructed a full, high-resolution spectral model of the leakage that was capable of handling any extended, diffuse spectrum that covers the entire field of view. This model is able to overcome the computational efficiency requirements; constructing a high-resolution exposure in ~ 12 hours. However, this comes at the cost of increased storage space. Additionally, we find that the model is able to correctly place leakage on the detector.

An assessment of the model’s accuracy reveals an oscillating trend. In regions where leakage is higher, the model is within 20% of comparable cryo-vacuum testing exposures, whereas in regions where the leakage is lower, the accuracy drops to within 50%, at times exceeding this. This oscillation is likely attributable to the single scale factor applied to each shutter not being sufficient to represent them. An improved scaling approach, potentially with additional scalings per shutter is required. In addition, there are also regions of generally higher over-subtraction, occurring due to a portion of micro-shutters being poorly modelled. These poorly modelled shutters require further investigation, and a strategy must be devised to accurately map the structure of leakage within them. A potential approach would be using a statistical criterion to identify them, and then attempt to find a common leakage structure to them.

For the case of NIRSpec’s gratings, in comparing the spectra generated by the model to those found in the corresponding testing exposures, we find the modelled spectra underestimate the true spectra. In this work,

a rudimentary first-order correction was applied. However, a deeper investigation into the root causes of this discrepancy is required.

Finally, once the causes of inaccuracies in the model have been addressed, there is scope for the model to be extended further. Primarily, given the high-resolution nature of the model, strategies could be implemented to modulate the model in order to account for the effects of grating wheel repositioning. Additionally, the model could also be expanded to handle multiple different spectra occurring at different spatial points.

6 REFERENCES

Deshpande, A. 2017, Assessing the Impact of the MSA Leakage on IFU Observations, Technical Note ESA-JWST-SCI-NRS-RP-2017-002, ESTEC

Dorner, B., Giardino, G., Ferruit, P., et al. 2016, *Astronomy & Astrophysics*, 592, A113

Lützendorf, N. 2017, Tracing the MSA leakage component common to all shutters, Technical Note ESA-JWST-SCI-NRS-TN-2017-051, STScI